# Methods to Determine Preferential Flow in Water Repellent Urban Soils

vorgelegt von:
M. Sc Math Al Hassane Diallo
aus Thies/Senegal

von der Fakultät VI der Technischen Universität Berlin
zur Erlangung des akademischen Grades

Doktor der Naturwissenschaften
Dr. rer. nat.
genehmigte Dissertation

Tag der wissenschaftlichen Aussprache: 23 März 2011

Promotionsausschuss:
Vorsitzender: Prof. Dr. M. Wilke
Berichter: Prof. Dr. Gerd Wessolek
Berichter: Prof. Dr. Heiko Diestel

Berlin 2011
D 83

## Table of Contents

**List of Table**



**List of Figure**

## Abstract

In literature, a wide range of approaches is described to characterize soil water repellency phenomena. The aim of this study is to detect preferential flow paths for two water repellent soils in an urban environment using various methods. The first experimental site is in “Berlin Buch”, a former wastewater disposal field, today’s covered dominantly by couch grass. The second site is in the “Tiergarten” park in the centre of Berlin. This site is covered by a short grass vegetation, which is cut regularly.

In this thesis, three methods were used and tested to analyze preferential flow paths due to water repellency.

- First, a tracer experiment with Brilliant Blue (well described in Flury and Flühler 1995) was applied to color the pathways of water infiltration. The soil was irrigated with 30 mm on the Tiergarten site and 50 mm water on the Buch site with a Brilliant Blue concentration of 1g/L. The water was distributed using a sprinkler system or a pesticide hand sprayer. After 24 hours, horizontal and vertical sections of the soil were excavated. A digital photo camera installed on a tripod was used to document the coloration of the soil. From the photos and water drop penetration tests the flow paths were detected.
- Second, a numerical model (DELPHIN) was used to analyze the influence of water repellency on surface temperature. The variation of initial water content, for example between dry and wet zones, can create different soil heat fluxes and consequently influence the surface temperature. The vegetation cover and the depths of the dry and wet areas influence the surface temperature. Thus, we analyzed only simplified heat and energy transport processes without any interaction of water and salt transport. The sensibility of the predictions was studied by varying the initial water content and depths of wet and dry areas of the soils. The spatial geometry of the model is a vertical sandy soil profile of one meter length and one meter depth without vegetation cover. In the first model concept, the wettable area is 4 cm wide and 40 cm depth. Two classes of sandy soil having the same physical properties but different water contents were used. In the second model the wet areas were larger (40 cm wide and 40 cm deep). The simulations ran for eight days. A standard data set offered by DELPHIN was used for the climatic conditions. The initial soil temperature was set to 15 °C.
- As a third method, a thermal camera was used for detecting soil surface temperature gradients induced by water repellent pattern. Experiment was done in the Tiergarten park during three sunny days in summer. In a water repellent soil, dry soil can exist next to zones of wet soil and the variation of initial water content between dry and wet zones can create a temperature gradient and can consequently influence the surface

temperature. This kind of soil design is found within the upper part of the soil profile. Several studies connected the heat balance at the soil surface to the physiological processes evapotranspiration and photosynthesis (Wiegand et al. 1983; Moran et al. 1994; Yuan et al. 2004). The advantages of the thermal infrared detection are fast and undisturbed measurements with high spatial resolution.

The **Brilliant Blue experiment** shows preferential flow paths. In the topsoil, it is possible to determine the spatial water repellency distribution from the Brilliant Blue images. Wettable areas are colored with Brilliant Blue, water repellent areas are not. Nevertheless, below 50 cm, where there is no presence of water repellent samples, the Brilliant Blue experiment showed preferential flow due to the gravitational flow of water. This preferential flow did not have any effect on the water content changes. These preferential flow paths, in their turn, manage the "hydraulic cycle" of the soil. Because water is the main transport medium of solutes, the preferential flow due to the water repellency in the topsoil also influences the solute transport in the soil.

**The numerical scenarios with Delphin 2D** showed that the size of the wettable area as well as the initial water content difference between wet and dry soils influenced the soil surface temperature, but not to a great extent. The covering depth of the wet or water repellent area has a higher influence on soil surface temperature differences than the thermal properties of the soil layer itself. It reduces the maximum between the differences in surface temperature of above the wet and dry spots in the soil. If the wet and dry spots were covered with more than 10 cm soil, the influence of the soil surface temperature was almost negligible. However, in natural soils, the vegetation cover has to be taken into account as well.

In a field experiment in Tiergarten park using the **thermal camera**, the surface temperatures during the day were up to 65°C with a very high spatial varaibility. Soil surface temperature structures were different during the day and during the night. The comparison between these structures and the spatial soil water content distribution did not give a good correspondence. It was not possible to detected wetter and dryer parts of the soil from the surface temperature. Nevertheless, water content and surface temperature were stasitically correlated at night. This can be explained by the higher importance of the soil heat flux during night.

## Zusammenfassung

In der Literatur sind viele unterschiedliche Ansätze zur Beschreibung von hydrophoben Bodeneigenschaften bekannt. Das Ziel der vorliegenden Arbeit ist es, präferenzielle Fließwege zu beschreiben. Dies erfolgte mit unterschiedlichen Methoden auf zwei urbanen Standorten mit benetzungsgehemmten Böden.
Der eine Standort ist ein ehemaliges Rieselfeld in Berlin Buch, der heute überwiegend mit Quecke bewachsen ist. Der andere ist eine Parkfläche mit Rasenbewuchs und liegt im Großen Tiergarten von Berlin.
In dieser Arbeit werden drei Methoden getestet um die präferenziellen Fließwege aufgrund von Benetzungshemmung zu beschreiben.

- Der erste Ansatz ist ein Tracer Experiment mit dem Farbstoff Brillant blue (s. Flury and Flühler, 1995). Dazu wurden die Versuchsflächen mit gefärbten Wasser beregnet; 30 mm wurden im Tiergarten und 50 mm in Buch aufgebracht; die Konzentration betrugt 1 mg/l. Nach 24 Stunden wurden die Flächen aufgegraben und an einer Profilwand horizontal und vertikal beprobt. Mit einer Digitalkamera wurde die Färbung des Bodens aufgenommen. Anhand der Photos in Verbindung mit Messungen der Benetzungshemmung (WDPT= water drop penetration time test) wurden die Fließwege im Boden bestimmt.
- Als zweite Methode wurde ein numerisches Simulationsmodell (DELPHIN) benutzt, um die Oberflächentemperatur in Abhängigkeit der Benetzungshemmung des Bodens zu analysieren. Die Unterschiede der Bodenwassergehalte zwischen feuchten und trockenen Bereichen führen zu unterschiedlichen Bodenwärmeströmen und beeinflussen somit die Oberflächentemperatur als Bestimmungsgröße.Ein Problen dabei ist, dass auch die Pflanzendecke und die Tiefe der feuchten und trockenen Bereiche im Boden die Oberflächentemperatur beeinflussen. Mit dem Simulationsmodell wurden vereinfachte Szenarien ohne Salztransport und Wasserfluss berechnet. Die Sensibilität der Berechnungen wurde durch Variation der Wassergehalte sowie durch unterschiedliche Tiefen der Trocken- und Feuchtezonen getestet. Das Modell zeichnete ein vertikales Sandprofil von 1m Länge und 1m Tiefe ohne Pflanzenbewuchs nach. In einem ersten Modellszenario waren die feuchten, benetzbaren Bereiche 4 cm breit und 40 cm tief; in einem zweiten Szenario wurde die Breite auf 40 cm erhöht. Die Simulationszeit umfasste einen Zeitraum von acht Tagen. Als klimatische Randbedingungen wurde ein Datensatz von DELPHIN verwendet; die Anfangstemperatur des Bodens betrug 15 °C.
- Als dritte Methode wurde eine Thermalkamera zur Dedektion von benetzungsbehemmten Bereichen (aus der Oberflächentemperatur) benutzt. Die

Experimente wurden an drei austauscharmen Strahlungstagen im Sommer im Tiergarten durchgeführt. In einem bentzungsgehemmten Boden können zeitgleich nebeneinader trockene und feuchte Bereiche existieren, die unterschiedliche Temperaturgradienten erzeugen und die Oberflächentemperatur beeinflussen.
Viele Studien verbinden die Energiebilanz an der Bodenoberfläche mit den pflanzenphysiolgischen Prozessen der Transpiration und Photosyntese (Wiegand et al, 1983, Moran et al., 1994, Yuan et al. 2004). Der Vorteil der Thermalbildkamera ist eine schnelle Messung mit hoher räumlicher Auflösung.

Das **Brillant blue Experiment** bildet die unterschiedlichen Fließwege deutlich ab. Im Oberboden konnte eine enge Beziehung zwischen der räumlichen Verteilungen von Brillant blue und der Benetzungshemmung festgestellt werden. Benetzbare Bereiche waren gefärbt, benetzungsgehemmte dagegen nicht. Unterhalb von 50 cm Bodentiefe, wo keine Benetzungshemmung mehr auftrat, zeigte das Tracerexperiment ebenfalls präferenzielles Fließen, was nicht direkt durch Benetzungshemmung erklärt werden kann. Dieser präferenzielle Fluss führte allerdings nicht mehr zu messbaren Wassergehaltsänderungen im Untergrund. Von dem präferenziellen Wasserfluss aufgrund der Benetzungshemmung sind natürlich auch alle Stofftransportvorgänge (gelöster Stoffe) betroffen.

Die numerischen Berechnungen mit DELPHIN 2D zeigen, dass die Größe der benetzbaren Bereiche wie auch die Wassergehaltsunterschiede zwischen feuchten und trockenen Böden einen Einfluss auf die Oberflächentemperatur ausüben. Dieser ist allerdinsg deutlich geringer als der Einfluss der Bodentiefe, in der die trockenen bzw. feuchten Bereiche beginnen. Je tiefer sich diese Bereiche befinden, desto geringer fallen die Unterschiede der Temperatur an der Bodenoberfläche aus. Liegen diese Bereiche tiefer als 10 cm im Boden, werden diese Unterschiede nahezu gänzlich verwischt.Unter natürlichen bedingungen muss zusätzlich der Effekt einer Pflanzendecke berücksichtigt werden.

Die Aufnahmen der Thermalbildkamera zeigen, dass während der sommerlichen Messperiode tagsüber Bodenoberflächentemperaturen von mehr 60 °C auftreten können, die einer großen kleinräumlichen Variabilität unterliegen. Die resultierenden Temperaturstrukturen sind tagsüber völlig anderer Art als während der Nacht. Ein Vergleich der beiden Temperaturstrukturen mit den Strukturen der Wassergehaltsverteilung ergab allerdings keinen plausiblen Zusammenhang, d.h. es war nicht ohne weiteres möglich, anhand der Oberflächentemperaturverteilung des Bodens auf die Bodenfeuchteverteilung zu schließen. Immerhin konnte für den Nachtzyklus ein signifikanter Einfluss der Wassergehalte

im Boden auf die Oberflächentemperatur aufgezeigt werden. Dieser Befund wird mit dem während der Nacht aufwärts gerichteten Bodenwärmestrom erklärt.

**Danksagung**

La redaction d'une these n'est pas une chose facile, néanmoins je réalise la chance que j'ai eu en travaillant à la TU Berlin auprès du Pr. Wessolek.qui n'a pas hésité à faire confiance à un étudiant africain malgré toutes les difficultés inhérentes. Il a su à la fois prodiguer ses conseils, son expérience et m'accorder la liberté nécessaire à la réalisation de tout travail de recherche. J'ai apprecié et admiré sa rigueur de pensée, sa simplicité et sa patience.Enfin à l'heure cruciale de la rédaction sa confiance et son aide financière m'ont aidé à surmonter cette dure épreuve. Je vous en suis très reconnaissant

Je remercie très chaleuereusement Pr. Diestel, co-directeur de cette thèse pour sa disponibilté et sa confiance qu'il m'a temoignée.

Ce travail n'aurait pas vu le jour sans le soutien spirituel et moral de Heiner Stoffregen et de sa femme Conny. Pour les 300 lundis matins où on a cohabité, où on s'est régulierement vu et entretenu sur mon travail de recherche,et où durant lesquels tu as supporté stoiquement les oscillations de mon moral, pour ta disponibilité, ta confiance, tes encouragements, ton sens organisé du travail, ta rigueur, ta simplicité, et ta patience à mon égard durant tout mon séjour, je t'en serai reconnaissant à vie.

Un grand Merci à Helena Schmieschek et Mickael Falcklam pour leurs conseils et aides aussi bien technique que morale tout au long de mon séjour , et à Beate Mc Kiffer et Christine pour avoir de temps en temps su m'encourager

Un merci particulier aux «Neukölln'hain Block» à savoir Thomas, Björn, Steffen, Leif, Peter, pour leurs conseils, leurs soutiens et leur bonne humeur qui ont contribué à rendre mon séjour très agréable.

Merci également aux thesards et aux stagiaires que j'ai eue la chance de rencontrer: Yong Nam, Alex, Peter, Eva, Gerd, Stefan, Beate, Katharina

Merci à mes compagnons de berlin qui ont su me faire évader de temps en temps de la rédaction: je me risque à citer des noms dans le désordre Svetlana, Dominik, Jasmin, Micha,

Suzanne, Suzi, Annnette, Charlie, Fady, Merdan,Chico, Frank, Enock, Patrice, Lamin, Muri, Ricky, Teddy, Mike

Ces remerciements seraient incomplets si ma famille n'y était associée. Merci donc à mon père, qui a tant voulu cette thèse, à ma mère, à mes sœurs et bien évidemment à mon frère jumeaux qui me manque tant. Ce travail vous est dedié

Enfin à tous ceux dont le nom m'échappe à cet instant et que je regretterai de n'avoir pas cités, tous mes remerciements

**List of Symbols**

| | | |
|---|---|---|
| $C$ | Volumetric heat capacity | [J/m³.K] |
| $Q$ | Heat content per unit of total volume | [J/m³] |
| $\rho$ | Density | [kg/m³] |
| $C_p$ | Isobar mass heat capacity | [J/Kg.K] |
| $C_{p,Soil}$ | Isobar soil heat capacity | [J/Kg.K] |
| $C_{\rho W}$ | isobar mass heat capacity of the water fraction | [J/Kg.K] |
| $C_{\rho S}$ | isobar mass heat capacity of the solid fraction | [J/Kg.K] |
| $C_{\rho a}$ | Isobar mass heat capacity of the air | [J/(m³ K)] |
| $\theta_a$ | Voluminal air fraction | [m³/m³] |
| $J_T$ | total flux of sensible heat | [J/m²s] |
| $J_\lambda$ | sensible heat flux transferred by thermal | [W/m²] |
| $J_S$ | sensible heat flux transferred by thermal convection | [W/m²] |
| $\lambda_i$ | Thermal Conductivity | [J/msK] |
| $\delta_T$ | Heat quantity exchanged during this process | |
| $\theta$ | Water content | [m³/m³] |
| $\rho_a$ | Air density | [kg/m³] |
| $D_T$ | Molecular diffusivity of thermodiffusion | [m²/s] |
| $\nu_{vap}$ | Gas voluminal fraction | |
| $D_e$ | Exchange coefficient | [m²/s] |
| $q_{vap}$ ´ | Volume flow per unit area | [m/s] |
| $\lambda_E$ | Latent heat of vaporization | [N/m²K] |
| $\varepsilon$ | Ratio of the vapor molecular weight to that of the air and of $\gamma$ | |
| $R_n$ | Net radiation | [W/m²] |
| *PM* | Radiative energy absorbed by the system for photosynthesis | [W/m²] |
| $\Delta S$ | Radiative energy converted into heat and stored in the system | [W/m²] |
| C | sensible heat | [W/m²] |
| $\lambda_E$ | Latent heat | [W/m²] |

| | | |
|---|---|---|
| $W_{\lambda b}$ | Radiation of a black body to the wavelength | [$Wm^{-2}\mu m^{-1}$] |
| $\lambda$ | Wavelength | [m] |
| $\lambda_{max}$ | Wavelength corresponding to the maximum of radiation | [m] |
| M | body exitance | [$Wm^{-2}$] |
| $M_b$ | Black body exitance | [$Wm^{-2}$] |
| $\sigma$ | stefan-Boltzmann constant $5{,}67032.10^{-8}$ | [$Wm^{-2}K^{-4}$] |
| $c$ | Speed of light: $3x10^{8}$ | [$m.s^{-1}$] |
| $h$ | Planck's constant : $6.63x10^{-34}$ | [Js] |
| $k$ | Boltzmann's constant : $1.38x10^{-23}$ | [$J.K^{-1}$] |
| $T$ | Temperature | [K] |
| $\varepsilon$ | Emissivity | |
| $f_c$ | Vegetationcover fraction | |
| $T_s$ | Surface temperature | [°C] |
| $T_c$ | Vegetationcover temperature | [°C] |
| $T_0$ | Soil temperature | [°C] |
| $\sigma$ | Standard deviation | |
| $T_H$ | Temperature of the wet thermometer | [K] |
| $T_a$ | Temperature of the dry thermometer | [K] |
| $e(T_H)$ | Vapor tension saturated at the temperature with the wet thermometer | [K] |
| $\gamma$ | Psychometric coefficient: 66 | [Pa/K] |
| F | Attraction force between two electric charges | [N] |
| $\varepsilon$ | Permittivity | |
| $Q_1$, $Q_2$ | Loads separated by a distance r in a uniform medium | [C] |
| $\mu_r$ | Magnetic permeability: it is equal to 1 for nonmagnetic materials | |
| CTV | Canopy Temperature Variability | |

# 1. Detecting Water Repellency Using Brilliant Blue as Tracer

## *1.1. Introduction*

Many soils of the world are water repellent. The soil exhibiting water repellency is found within the upper part of the soil profile. Field observations have indicated that the rates of water infiltration into these soils are greatly affected by these surface conditions. The aim of our study was to detect preferential flow paths for two water repellent soils in an urban environment using various methods. One site is “Berlin Buch”, a former waste water disposal field, the second one is the park “Tiergarten” in the centre of Berlin.

In literature a wide range of approaches was used to characterize water repellency. Specific techniques were evaluated, included using intrinsic sorptivity as an index for assessing water repellency (Wallis et al. 1991) and standardizing the "water drop penetration time" and the "molarity of an ethanol droplet" techniques to classify soil hydrophobicity (Doerr 1998). A need to better designate the differences between "potential"´and "actual" water repellency and to establish a "critical soil water content" when assessing water repellency was identfied (Dekker and Ritsema 1994) The water repellency of an oven-dried sample is designated as "potential" , in contrast to the water repellency of a field moist sample which is referred to as "actual".

In this study three methods were used and tested to determine preferenetial flow paths: first a tracer experiment with brilliant blue which is a cheap, non-toxic, easy to handle and well described tracer (Flury and Flùhler 1995). Second a numerical model was used to analyse the influence of water repellency on surface temperature. Third a experimetal setup using a thermal camera for detecting surface temperature indicating water repellent spots for a water repellent lawn.

Thus this thesis is organized within three chapters according to the above mentioned methods. The following chapter 1 starts with a short review on literature on water repellency.

The aim of this chapter is to compare the water drop penetration time test with the Brilliant Blue tracer. Moreover it should be tested whether a correlation between the water drop penetration tiime test and the Brilliant Blue results exists in order to determine the spatial water repellency distribution from Brilliant Blue images. A short overview is given first on the origin of water repellency, following by standard methods for the characterisation of Water repellency and at least an introduction in tracer studies used in soil physics.

## *1.2. Descriptive Literature*

### Origin of Water Repellency

Interest in water repellency phenomena began well before the 20th century. An examination of the literature before 1900 indicates that water repellency was mostly associated with observations on organic matter and its decomposition, particularly where fungi were involved. And none of these pre-20th century publications used the term "water repellent".

In 1910, during their investigations of humic substances in a California soil, Schreiner and Shorey reported a soil that "could not be wetted, either by man, by rain, irrigation or movement of water from the subsoil". In 1911, Bayliss validated that soils containing mycelium were difficult to wet and cited an example where rain did not penetrate the soil in mycelia areas but penetrated to a depth of 10cm in the adjacent non-mycelial areas.

Between 1920 and 1939 only 2 publications were found that discussed water repellency. These were : a report of resistance to wetting in sand (Albert and Köhn, 1926) and a second report describing the creation of "ironclad" catchments (Kenyon, 1929).

Between 1940 and 1959, published papers reporting observations on water-repellent soils began appearing in several scientific journals. Van't Woudt (1959) reported that organic particles coatings are affecting the wettability of soils in New Zeland. Also water repellency was not specifically mentioned as being a factor in aggregate stability. An interest in characterizing contact angles also began emerging (Bikerman, 1941). Water repellency was also starting to be utilized for beneficial uses, including its use for water harvesting where paved drainage basins provided a source of water livestock or game (Humphrey and Shaw 1957), its application as moisture, thermal and electric insulator during highway construction (Kolyasev and Holodov, 1958), and its potential for decreasing soil water evaporation(Lemon, 1956).

The accumulation of knowledge about water repellency and its treatment had accumulated to such an extent. During the 1960s numerical publications also appeared that contributed fundamental knowledge in fields related to water repellency. A comprehensive synthesis of information on the dynamics of aggregation was published (Harris et al. 1966) in addition to a classification of aggregates based on their coherence in water (Emerson, 1967).

During 1970s, the interest in water repellency and its management implications began to attract worldwide attention. All over the world, water repellency was reported in: USA, Australia, Egypt (Bishay and Bakhati, 1976), in Japan (Nakaya et al., 1977a), in Nepal (Chakrabarti, 1971), in Mali (Rietveld 1978) and new Zeland (John, 1978). Other additional research continued to be conducted on: using wetting agents for remedial treatments (Letey 1975, Debano and Rice, 1973 etc), fire induced water repellency (Debano et al., 1976),

characterizing water repellency (Bahrani et al.,1970; Watson et Letey, 1970, Philip, 1971) and soil water movement (Debano, 1975, Hiller and Berliner, 1974). Important theorical efforts by soil physicists began identifying more realistic models for describing soil water movement in water repellent systems (Philip, 1975b, Mualem 1974).

The decade starting in 1980 was characterized not only by continuing strong interest in water repellency all over the world in Australia (Ma'shum and Farmer, 1985), Poland (Prusinkiewicz and Kosakowski, 1986) and in USA (Taylor and Blake, 1982) but also saw the development of knowledge in related areas which will be used during 1990s as the basis for describing water movement in hard-to-wet soils and which are: surface hydrology (Zaslavsky and Sinai, 1981), integrated soil water systems (Dekker and Bouma 1984). Several areas of water repellency studied during the 1960s and 1970s continued to attract interest during the 1980s. These include: fire-induced water repellency (Wells, 1987; Henderson and Golding; 1983; Scott, 1988;), characterizing water repellency (Richardson, 1984; Tillman et al., 1989,), and the effect of water repellency on soil water movement (Hendrickx et al., 1988b).After 1990, the role of water repellency within the context of environmental management is examined (De Rooij and de Vries, 1996). In addition, significant papers appeared which described theorical models on fingering and instability of wetting fronts (Dekker and Ritsema 1994; Dekker and Ritsema 1995; Dekker and Ritsema 1996; Dekker and Ritsema 1996; Dekker and Ritsema 1997; Ritsema and Dekker 1998, Hendrickx et al., 1993; Ritsema and Dekker 1996, van damm et al., 1996) and water movement through macropores in soils (Mallants et al., 1996).

**Methods for Characterising Water Repellency**

Between 1960 and 1969, physical methods for characterizing soil water-repellency were developed. In 1962, Letey and coworkers published 2 significant papers, one describing the measurment of liquid-solid contact angles in soil and sand (Letey and al., 1962a), and a second describing the influence of water-solid contact angles on water movement in soil (Letey et al., 1962b). These publications were followed in 1968 by a publication by Letey who described a method to measure water repellency: the water drop penetration time test. This method can be used on field moist samples for the actual repellency or dried samples for the potential repellency. With the aid of this test dry repellent soil samples can be separated from wet non repellent ones. Three drops of distilled water from a standard medicine dropper are placed on the smoothed surface of a soil sample, and the time that elapses before the drops are absorbed is determined. The Table 1.1 shows the water drop penetration time classes. A soil is considered to be water repellent if the WDPT exceed 5 s (Bond, 1964). Based on this method, Debano classified the Holland soils into five repellency classes: (1) wettable soil for

WDPT < 5s; (2) slightly water repellent soil for WDPT =5-60s; (3) strongly water repellent soil for WDPT =60-600s; (4) severely water repellent soil for WDPT=600-3600s; (5 and 6) extremely water repellent soil for WDPT >3600s.

Table1.1: WDPT classes

| Class | WDPT |
|---|---|
| 6 | > 6 h |
| 5 | 3-6 h |
| 4 | 1-3 h |
| 3 | 10-60 min |
| 2 | 1-10 min |
| 1 | 5-60 sec |
| 0 | wettable |

**Tracer Experiments**

Various tracer experiments have been carried out in soil science to mark preferential flow paths. Conservative tracers like bromide and chloride have been used as well as dye or fluorescence tracers. One disadvantage of dye tracers is the temporal decay of the tracer. Therefore, most of the shorter experiments with irrigation have been carried out using dye tracers (Vanderborght et al., 2002; Forrer et al., 2000), while in long term experiments inorganic anions like bromide or chloride predominate (Dyck, 2003; Kohne et al., 2005; Hammel et al., 1999). Bromide is the most suitable tracer in the group of inorganic anions (Flury and Wai, 2003), because of its low concentration in natural soils. Ritsema and Dekker (1998) conducted tracer experiments to mark preferential flow paths in water repellent soils.

Multi-tracer experiments were used in several studies (Kung et al., 2000; Kasteel et al., 2003; Koschinski et al., 2006). Hangen et al. (2005) applied a tracer cocktail consisting of bromide, terbuthylazine, and deuterium to the soil surface of a potentially water repellent lime soil and subjected it to natural infiltration. Tracer concentrations in drainage waters were analyzed for a period of about 10 months. They determined a sectional drainage area in 110 cm depth of 71% in spring and 35% in autumn. The results for bromide and deuterium were comparable; the absence of terbuthylazine indicates the absence of rapid flow in the soil. Several authors showed that bromide is adsorbed slightly in the soil (Brooks et al., 1998; Clay et al., 2004).

Several new analytical and visualization techniques were reported which could potentially improve the assesment of water repellency and its effect on soil water movement. One such technique is the use of computed tomographs as a tool for non-destructive analysis of flow patterns in macroporous clay (Heijs, De Lange et al. 1995). Time Domain reflectometry employing standard three-rod probes was also used to measure volumetric water contents at

different times and positions in the soil profile (Ritsema et al., 1997a). Visualization techniques, useful for more vividly portraying three-dimensional finger flow patterns, was generated using modular visualization software and associated computer hardware (Heijs, Ritsema et al. 1996). Extraction of samples from the soil and the associated chemical analysis in the required spatial solution can be costly.

Dye tracer experiments have recently become increasingly popular to visualize the heterogeneous nature of flow and transport pathways at the field plot scale (Clarke et al. 2000, Nielsen et al. 1997, Öhrström et al. 2004, Dekker et al. 2000). Images of stained soil profiles can easily be classified into stained and unstained areas using image analysis. This allows a semi-quantitative measure of the flow patterns, the so-called dye coverage (Hangen et al. 2001, Kasteel et al. 2000, Vogel et al. 2002).

The food dye Brilliant Blue FCF (Color Index 42090) was previously used by Burkhardt et al. 2002 to determine absolute concentrations in small-scale field plots with a pixel resolution of 1 $mm^2$ using image analysis procedures. The resident concentration of the dye in their study was estimated using a second-order polynomial regression with depth and the primary colors red, green, and blue as the explanatory variables. This method appears very promising for analyzing high spatial resolution flow and transport processes in the vadose zone. Simultaneous application of Brilliant Blue with a conservative tracer that follows the water flow pathways may provide a very detailed description of solute transport, as shown by Täumer et al. 2005 and Van't Woudt. et al. 1959 among others.

## *1.3. Materials and Methods*

### *1.3.1. Study Site Berlin-Buch*

Berlin Buch is located at the northern city limit of Berlin (49°29'31" north, 11°02'59" east) was drained nearly 100 years long by unsettled waste water and from 1965 to the cessation of this drainage in the year 1985, up to 10.000 mm/ year of waste water were discharged. In the year 1985 in the course of the 750 year celebration of the city Berlin a transformation of this large surface in leisure and a recovery landscape was undertaken. Today sandy output sediments Regosole with at on average 15-60 cm (partially till 100cm) powerful rich in humus horizons which exhibit high heavy metal and Organic charges find oneself on the poor clay. Below 45cm of the topsoil the soil is shaped by unweathered, strongly sandy, glaciofluvial material, which exhibits a very small CEC (cation exchange capacity) at acid pH values. The waste water infiltration of many years led to drastic changes of the soil characteristics. Material balances show on the one hand an accumulation of the organic soil substance and heavy metals and on the other hand, a iron and manganese depletion. After completion the locations remained are subject to the wastewater farm use until today strong conversion

dynamics in the topsoil. At altogether very high pollutant contents and droping pH values (acidification due to mineralization procedures) those take to heavy metal (SM) concentrations in the soil solution continuously too. Aluminium concentrations are measured already now of up to 100 mg/l in the soil solution. With concentrations over 20 mg/l toxic effects on the root system of trees are proven. As typical consequences after closing of the wastewater farm enterprise, damages of the cultivated tree appeared. This stress situation for plant growth is strengthened by, the long lasting dry periods typical for Berlin in the summer half-year. The highest layer loadings are in the Ah horizons and sewage sludge volumes; up to 90 % of the total amount, are in these ranges. The pollutant entries into the soil took place predominantly individually bound at organic waste water constituents. Therefore the close relationship between the organic content in the soil and the measured pollutant contents can be explained among other things. Sewage farms exhibit typical distribution samples for pollutants. In a first gallery are the highest pollutant concentrations in the introducing inheritance realm and decrease in the following basins. Organic content lies on the average for PCB with 3 mg/kg, for PAK with 4 mg/kg and for MKW with approximately 220 mg/kg. Untreated wastewater was applied on 13000 ha of sewage farm land around Berlin since 1890. In 1985 the wastewater application was stopped, the soil surface was levelled, and an effort was made to reforest the fields. Most of the trees died, mainly due to water shortage during summer time, nutrient deficiencies, and heavy metal contamination (Schlenther et al., 1996). The average air temperature of the site is 7.5ºC, and the yearly precipitation is 580 mm (340 mm in summer, 240 mm in winter). Today, dry grasslands (mainly couch grass: Elytrigia repens) can be found. Figure 1.1 shows a typical soil profil at Berlin-Buch. The soil, a hortic Anthrosol, consists of a 40 - 60 cm organic topsoil upon medium-sized sand. The organic matter content of the topsoil horizon ranges mainly between 0.04 and 0.06 g g -1, organic matter spots up to 0.3 g g -1. Below a depth of 40 cm it is approximately 0.01 g g -1, below 60cm it is lower than 0.005 g g -1. The clay content in the non-calcareous fluvial sand is less than 0.01g g -1. Due to the reforestation effort, the surface is slightly undulated (wavelength 3.3 m; amplitude 10-15 cm). Rapid turnover processes of organic matter occur and an increased leaching of heavy metals and nitrate were measured (Hoffmann, 2002).

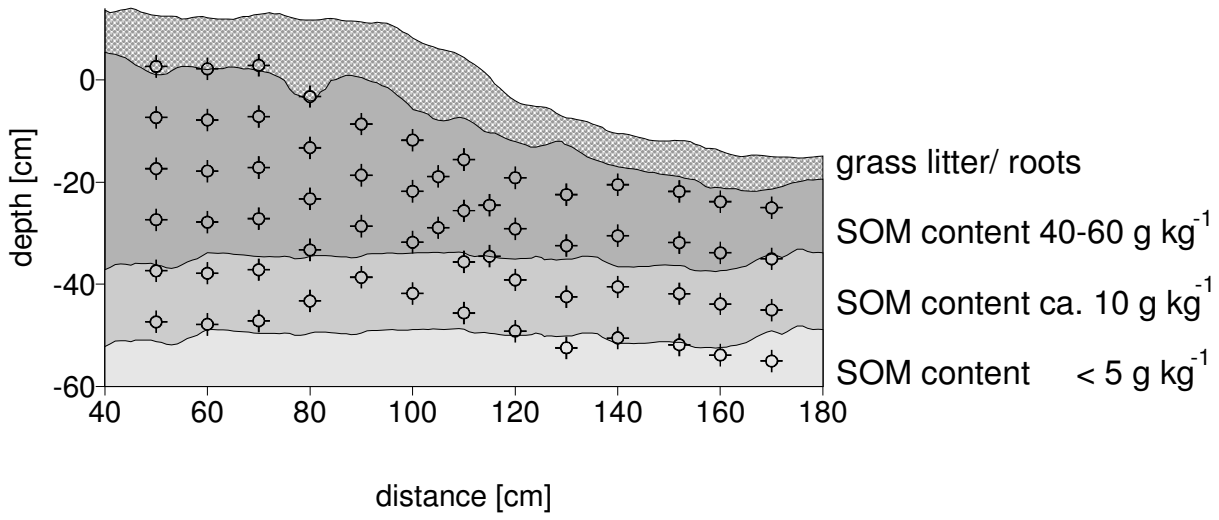


Figure 1.1: Soil organic matter (SOM) content distribution in Buch (Täumer, 2007)

Table 1.2: Selected physical and chemical soil properties in Buch and Particle size distribution (Kühn, 2001)

| Depth | Horizon | Sand | Silt | Clay | PH | C_org | Munsell |
|---|---|---|---|---|---|---|---|
| Cm | | % | % | % | $H_2O$ | (% g/g) | |
| 0-17 | Ah1 | 94,3 | 5,4 | 0,3 | 5,4 | 2,56 | 10YR3/2 |
| 17-25 | Ah2 | n.b | n.b | n.b | 6,1 | 20,41 | 10YR2/1 |
| 25-60 | Bv-rGo | 96,1 | 3,3 | 0,5 | 4,5 | 0,19 | 10YR5/4-5/6 |
| 60-165 | rGo | 91,9 | 7,4 | 0,7 | 4,3 | <0,09 | 10YR6/3-6/4 |

### *1.3.2. Field Investigations and Measurements*

The soil was preliminary irrigated on 12 m². We applied 50mm water with a Brilliant blue concentration of 1g/L by using a sprinkler system automated rainfall simulator. After 24 hours, horizontal sections of the soil were excavated. The pictures were taken with a digital photo camera. The camera was mounted on a special horizontal tripod construction which allowed adjusting the distance from camera to soil section similar for all photographs. So, the spatial information is the same for pictures from different depths.

Figure 1.2 shows the spatial arrangement of our transects in the field. We have two vertical profiles (Transect 1, transect 2) and between transects 1 and 2 we left 100 cm of distance between them (see Figure 1.2). Between these 2 transects horizontal cross sections of 1

meter width and 3m length parallel to the soil surface at 10 cm distances till 100 cm depth were prepared and photographed .

For each cross section, photographs were taken together with Kodak colour reference, a grey scale paperboard in the picture and a frame for geometrical and illumination correction of digital pictures. We used a reference line and a perpendicular to place the frame exactly in the same relative position in consecutive depths.

To estimate Brilliant Blue concentrations in the images from the colour spectra, a calibration against measured dye concentrations is needed. A thin layer of approximately 12 to 15 g of soil was scraped from homogeneously stained and unstained areas with different dye intensities. In total, 10 samples were taken in every cross sections. the sampling positions were randomly distributed across the plot. The sampling locations were marked and each cross section was recorded on separate photographs. Figure 1.3 shows the spatial arrangement of the samples on transect 1 and transect 2.

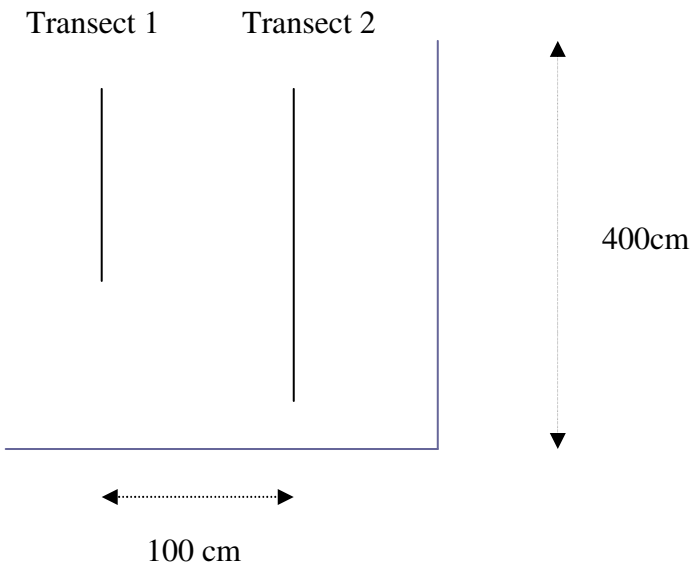


Figure 1.2: Spatial arrangement of the transects in the field

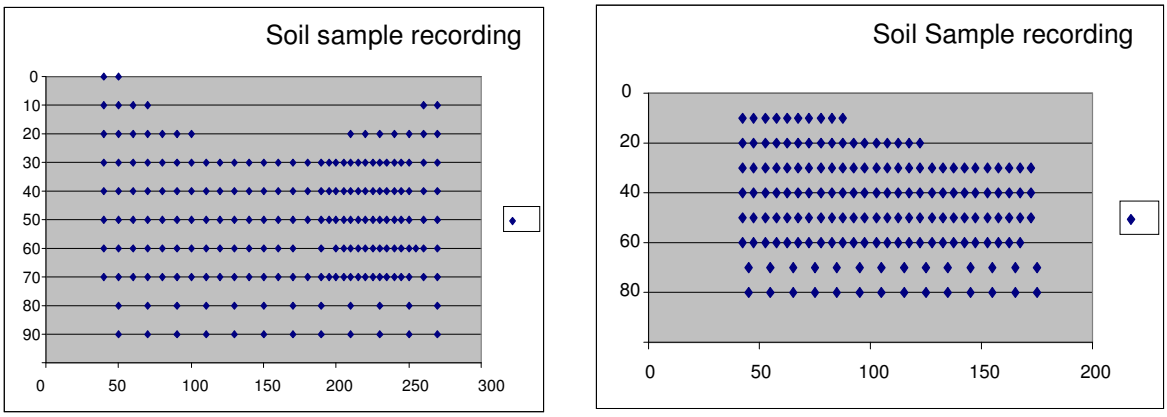


Figure 1.3: Soil sampling spatial resolution on the transects 1 (left) and on 2 (right) in Buch

### *1.3.3. Laboratory Measurments*

For the extraction of Brilliant Blue, 1 g of oven-dried soil (105°C) soil was equilibrated with 50 ml of a (4:1) water and acetone solution by shaking for 10 minutes. The suspension was centrifuged for 20 minutes and was collected. The extraction procedure was repeated 3 times. Then the suspension was equilibrated at 250 ml with the water-acetone solution. And 20ml of the solution were collected to measure the Brilliant Blue concentration with a photo spectrometer.

The spatial water repellency distribution was determined with the Water Drop Penetration Time (WDPT) test and according to the scale established previously in Table 1.1. Three drops of distilled water were placed on the smoothed surface of a field moist soil sample using a standard medicine dropper. The time that elapsed before the drops were absorbed was measured.

The water content of all samples was determined gravimetrically by drying at 105° C.

Afterwards the dry samples were used to measure the content of organic matter by igniting the samples for 5h at 550°C. The difference between the dried and ignited samples was taken as the organic matter content.

### *1.3.4. Image Processing Procedure*

Digital image processing has been used as a valuable tool for the analysis of dye tracer experiments in both, laboratory and field studies (Forrer et al., 1999; Kildsgaard and Engesgaard, 2002). The distinction of dye stained and through flown pixels from unstained and not through-flown regions by an explicit, objective and reproducible method is an important step of analyzing. If the contrast between the unstained soil and the dye stained soil region is high, this step might be easy. Obviously, the information content of stained regions is limited in dark soil regions, or if soil and dye tracers emit light in similar wavelengths. The chaotic mixture of light and dark colored soil regions is a characteristic of water repellent soils. It is a major barrier for the distinction of dye stained pixels from unstained pixels in digital image processing. A digital image processing method has been developed, which can extract dye tracer information from images of heterogeneously colored soils.

We used a well established method (Nehls et al., 2006), developed for arable soils, to investigate the flow paths in urban soils. For the image processing, the images were corrected for geometrical distortion. That includes first, the spatial transformation of pixels using the tie point concept and second, the gray-level interpolation (Gonzalez and Woods, 2002).The resulting images show the same combination of red, green and blue reflectance values (RGB) for the same colour. So one pixel represents a quadratic soil area of 54 $cm^2$. this image processing step is programmed using the programming language package IDL, version 6.0 (Interactive Data Language, Research Systems, Inc., Boulder, CO, USA). Each pixel represents not only the tracer intensity, but also the background color of the soil. Due to mixture of soil and tracer colors one discern a wide range of different blue intensities. Detecting "stained" pixels therefore requires separation of soil colors and dye tracer intensities. When displayed in the RGB colour model, the red channel shows the highest Brilliant Blue reflectance, while the blue channel contains almost no tracer intensities but contains the soil color information. That's why we choose the red channel to detect stained pixels (dark pixels).

Unstained pixels (light pixels) can be excluded as well, as long as no stained pixel (dark pixels) remains.

A threshold was used to separate out the dyed area of the soil in order to perform a percentage stain analysis. The colour threshold values determined in red channel were 80-160.

## *1.4. Results and Discussion*

### *1.4.1. Water Content, Organic Matter Content and Water Repellency Spatial Distribution*

Figure 1.7 shows the organic matter content spatial distribution on the transect 1. In this transect the organic matter content falls sharply in the first 40 cm to pass from 0,11 (g/g) to 0,04 (g/g) . From 40 cm of depth and on the remainder of the profile, it continues to decrease but in a way slower till 0,02 (g/g).

In transect 2, several tendencies are dissociated; between the surface and 40 cm depth, the evolution is similar to that of the transect 1 but the fall of organic matter content however is slower: it passes from 0,12 (g/g) to 0,08 (g/g). Thus, the transect 2 is richer in organic matter in the first 40cm horizons, than the transect 1. Till 60 cm depth the organic matter content decreases till 0,02 (g/g) before it's stabilized till 80 cm depth.

Figures 1.4 and 1.5 show the water content and water repellency spatial distributions respectively on transects 1 and 2. The soil water content in this site lies between 0,04 and 0,21 (g/g). Between transects 1 and 2, the general evolution is not the same. In transect 2, in the top of the profile, close to the surface, voluminal moisture is close to 20 Vol.%. It decreases till 10 Vol.% then regularly until 80 cm depth. In transect 1, the space variation is marked definitely. On the soil surface, the water content is 0,17(g/g) and it increases until 40 cm depth, and then strongly decreases to exceed 0,12 (g/g) at 50 cm of depth. Below 50 cm depth, the water content decreases again till 0,10 (g/g) at 80cm depth.

Figure 1.6 shows the percentage of water repellent samples according the depth on the transect 1 and 2. Both data were similar and the degree of actual water repellency decreased according to the depth. In total 25% of the soil samples on the transect 2 were water repellent whereas they are approximately 30% on the transect 1. At 10 cm depth all the soil samples of the transect 1 were water repellent and only 60% on the transect 2. At 20cm depth all the soil samples on the transect 1 remain water repellent and 59% are water repellent on the transect 2. At depth 30cm and 40 cm, the percentage of water repellent soil samples decreases gradually from 59% to 36% for the transect 2 and from 93% to 43% for the transect 1. From 50cm no water repellent soil samples were observed in both profiles.

Figure 1.7 shows the organic matter content spatial distribution on transect 1. The organic matter content decreased with depth, independently of the flow pattern. The distribution of water repellency was not directly correlated to organic matter content, but areas without organic matter were not repellent. Although organic matter content is responsible for water repellency, it is not the amount, but the type of organic matter which seems to be important (Doerr et al., 2000). This was observed in the runoff of the transect 1 which had higher organic matter contents but was not actually water repellent (see Figures 1.5 and 1.7).

As Figure 1.5 shows for Buch, we find water repellency only in the Ah Horizon, precisely in the first 50 cm of the topsoil. On this layer, the water repellency spatial distribution is similar to h that of the water content. Also let us note that up to 40 cm of depth, the percentage of flow paths is appreciably equal to the percentage of water repellent samples. This means that from the WDPT test, one can directly deduce the flow path spatial distribution.

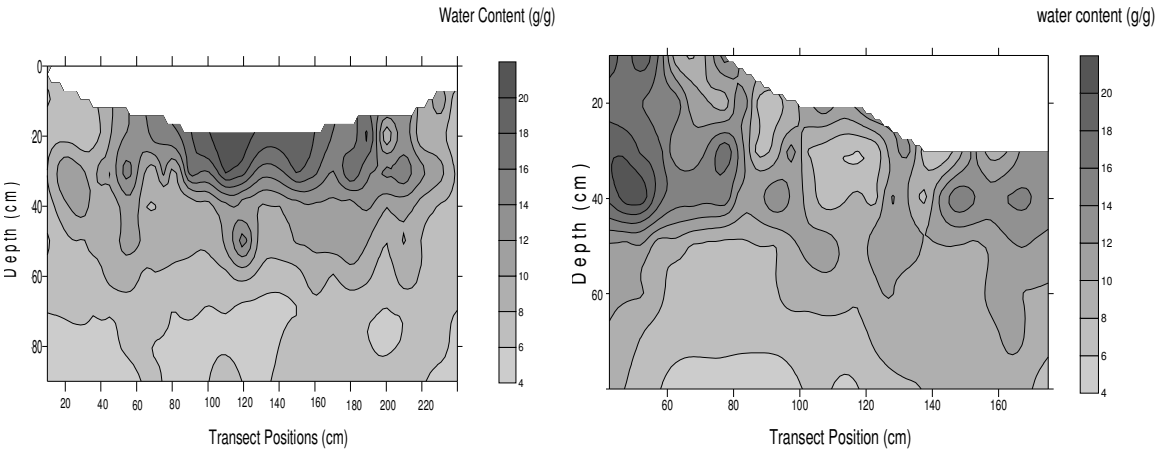


Figure 1.4: Gravimetric water content on transect 1 (left) and on transect 2 (right) Date: (November 25, 2006)

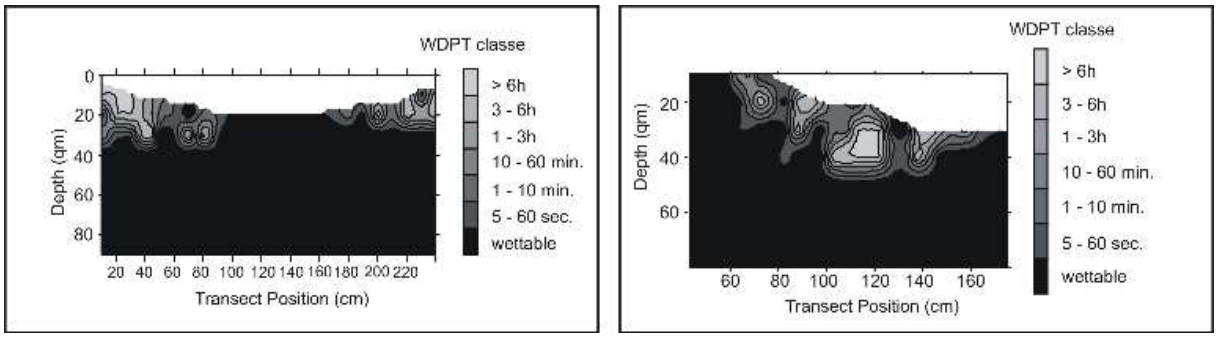


Figure 1.5: Water repellency spatial distribution on transect 1 (left) and on transect 2 (right) (November, 25, 2006)

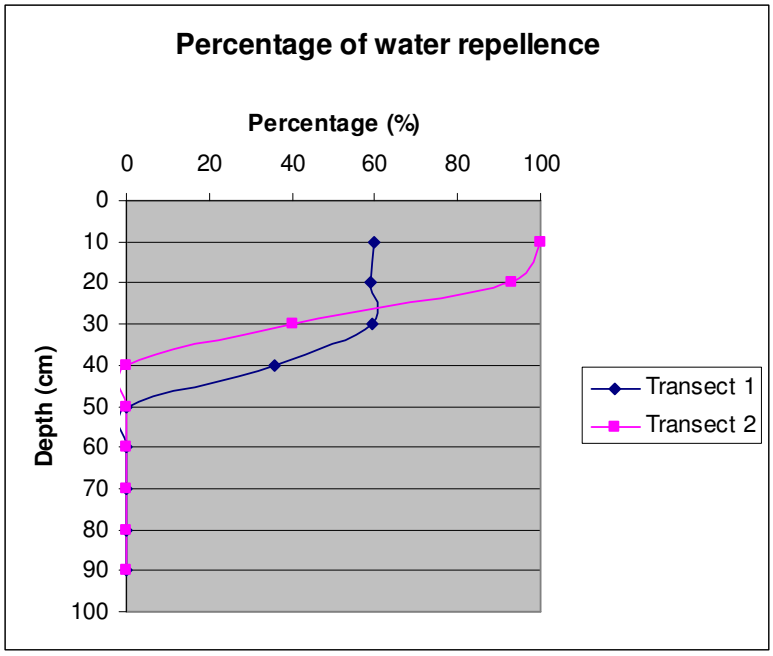


Figure 1.6: Percentage of water repellent samples according to the depth at transects 1 and 2 in Buch

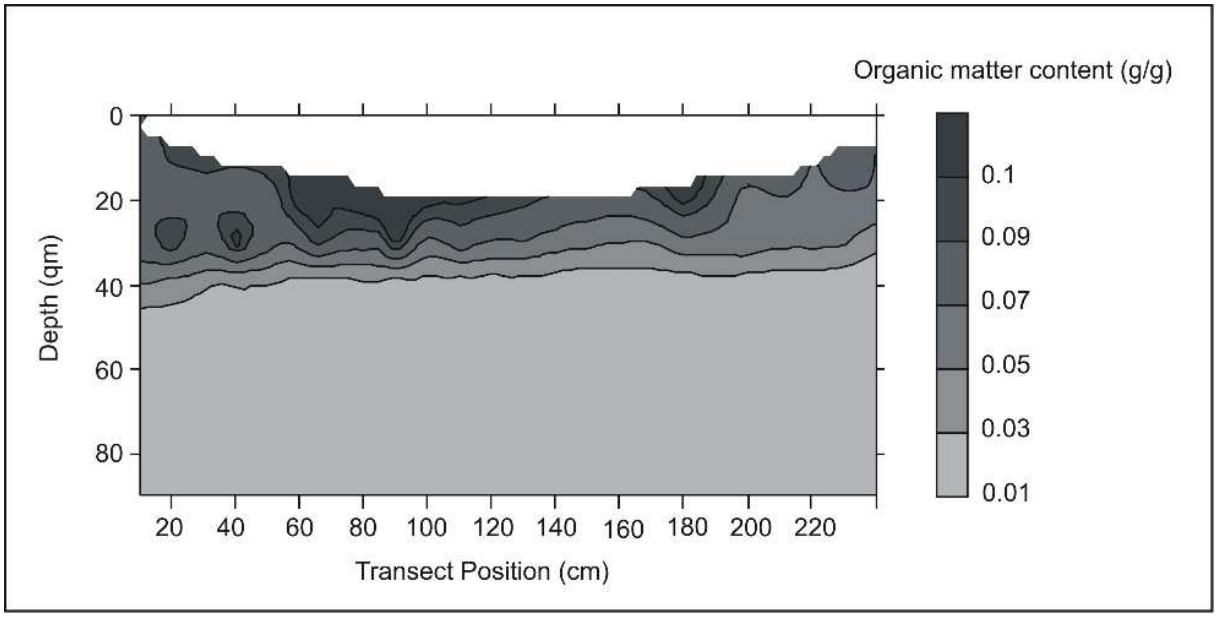


Figure 1.7: Organic matter content spatial distribution on transect 1 (November, 25, 2006)

### *1.4.2. Preferential Flow*

Figures 1.8 and 1.9 show the flow path percentages according the depth on the transect 1 before and after using the image processing procedure . The Brilliant blue experiment shows significant flow paths. The peak of the dye coverage was always found in the top of the

profile with the average depth of 40% dye coverage at 40 cm depth on the transect 1, and which corresponds to the same flow path percentage (percentage of stained pixels) of the horizontal cross section at the same level. A sharp decrease in stained area fraction was observed beyond 50 cm depth. Nevertheless below 50 cm, where there is no presence of water repellent samples, the Brilliant Blue experiment showed a preferential flow due to the gravitational flow of water. And this preferential flow did not have any effect on the water content changes.

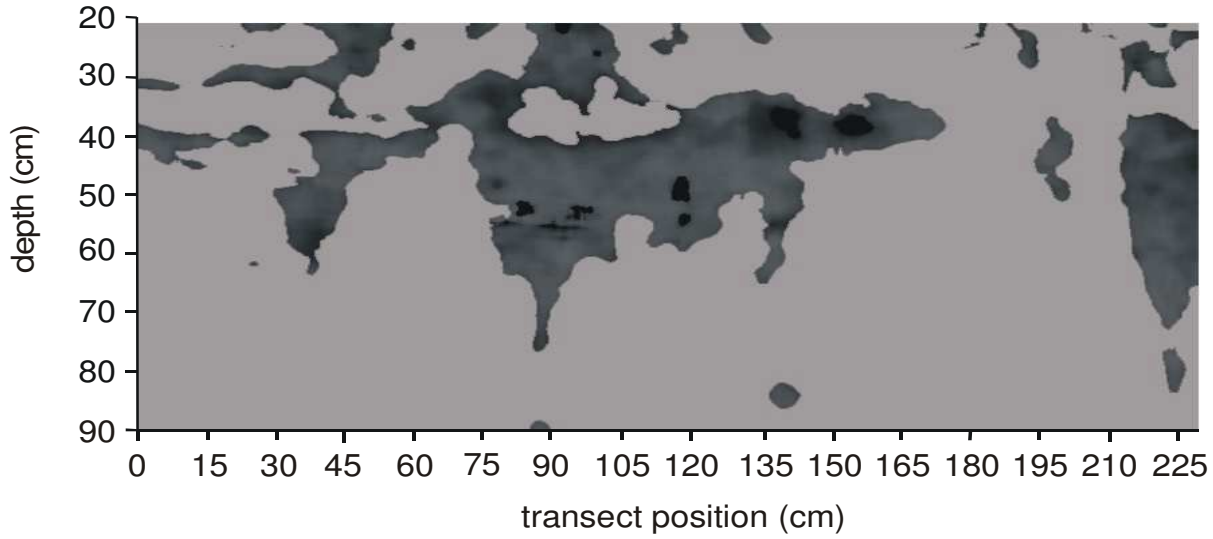


Figure 1.8: Flow path according the depth on the transect 1 in Buch

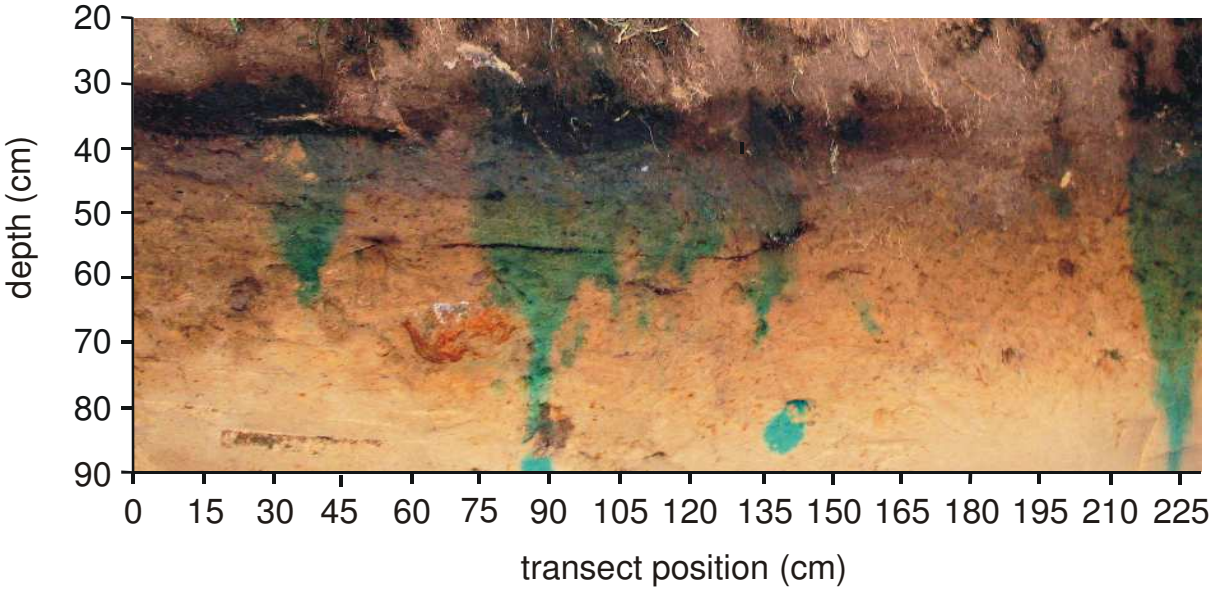


Figure 1.9: Flow path on the original transect 1 image in Buch

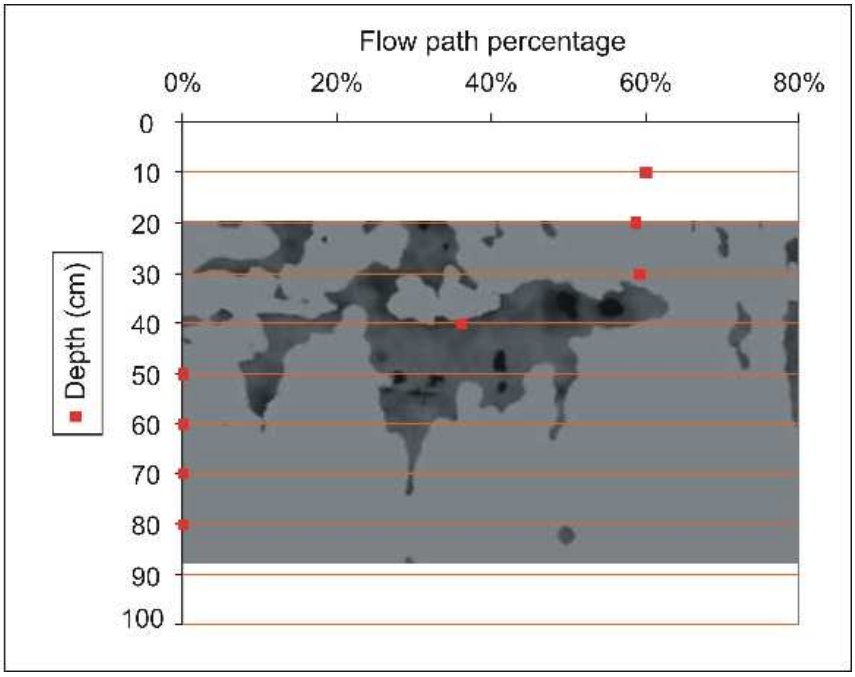


Figure 1.10: Flow path percentage according to the depth on the transect 1 in Buch

### *1.5. Conclusions*

The soil water content in Berlin-Buch lies between 0,04 and 0,21 (g/g). At this site, we find water repellency only in the Ah Horizon, precisely in the first 50 cm of the topsoil. The actual water repellency degree decreased according to the depth in both transects. In total 25-30% of all soil samples from transect 1 and 2 have been water repellent. On the relevant topsoil, the water repellency spatial distribution is similar with that of the water content. Also let us note that up to 40 cm of depth, the percentage of flow paths are appreciably equal to the percentage of water repellent samples. This means that from the WDPT test, one can directly deduce the flow path spatial distribution. The distribution of water repellency was not directly correlated to organic matter content, but areas without organic matter were not repellent.

The Brilliant blue experiment shows significant flow paths. In the topsoil, it is possible to determine the spatial water repellency distribution from the Brilliant Blue images

Nevertheless below 50 cm, where there is no presence of water repellent samples, the Brilliant Blue experiment showed a preferential flow due to the gravitational water flow (flow due to the gravitation). And this preferential flow did not have any effect on the water content changes.

These preferential flows, in their turn, manage the "hydraulic cycle" of the soil in the sense that they determine the quantity of rains water which be stored in the soil for the plants

(transpiration) or to restock the ground water or to drain and which be redirected to the atmosphere and to the soil surface.

In combination with further measurements the results can be used to detect the temporal dynamic of the spatial variability of water repellent areas. This will lead to a better understanding of the solute transport and water budget of water repellent sites.

## 2. Modelling Heat Transport using 2D- Delphin

### 2.1. Simulation Goal

The soil temperature present continual variations under the influence of the climatic conditions which determine the intensity of the energy exchanges between soil and atmosphere. The variations of the climatic conditions, and in particular the solar radiation intensity, happen in a relatively stable way according to periodic cycles, in particular on a daily scale and an annual scale. The soil thermal behaviour, which one can describe by the variations of his time dependent temperature profile, presents a similar cyclic behaviour consequently. The alternation of day and night, cloudy phases, storms, periods of dryness, the surge of cold or hot air, the evolution degree of the vegetation cover and the presence of water repellent areas, give rhythm to the soil thermal variation cycles. As in Figure 2.1, in a water repellent soil, dry soil can exist next to zones of wet soil and this is found within the upper part of the soil profile.

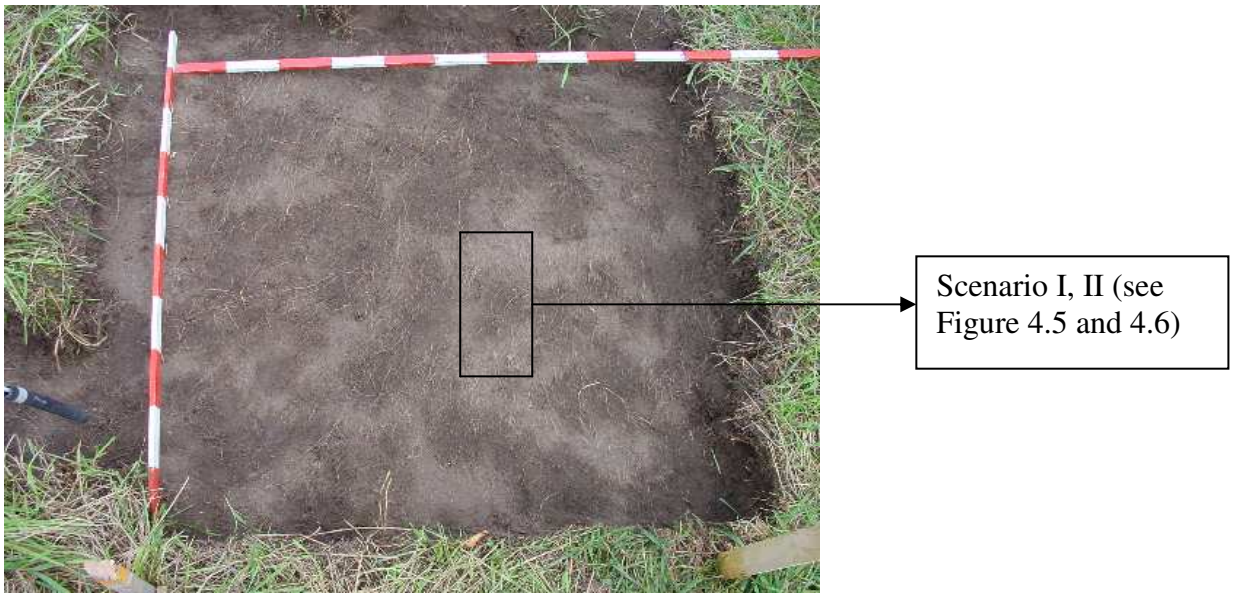


Figure 2.1: A typical water repellent spatial distribution with dark but wet zones and light but dry zones

The parameters implied in the surface temperature calculation, vary considerably in space and time. The variation of initial water content for example between dry and wet zones can create a temperature gradient and consequently can influence the surface temperature. The vegetation cover and the depth of these wet areas (the covering depth) also intervene in the surface temperature calculation. Thus this chapter will treat only simple heat and energies transport problems without any interaction with water and salt transport. We Will study then the sensibility of our models by initial water content variations between wet and dry soils and by covering depth variation of this wet soils on the Results.

## *2.2. Theory of Heat transport in Soil*

### *2.2.1. Soil Thermal Properties*

The heat transfers fall under the energy exchange context, which are: radiative energy, thermal energy and latent energy. Soil and vegetation, as a thermodynamic system, led to distinguish the external energy exchanges, of the internal exchanges. The internal exchange occur according to two different processes: thermal conduction and thermal convection. The principal parameters which intervene in soil thermal behaviour are those which make it possible to characterize, on the quantitative and capacitive level, the thermal heat which it stored. The soils thermal properties are conditioned by the characteristics ones of their texture and their structure.

**Heat capacity**

The heat capacity C of a body is defined by the ratio *dQ/dT* where dQ represents thermal heat necessary to raise the temperature of this body by dT (André Musy et Marc Soutter). The isobar mass heat thermal capacity Cp represents the heat storage capacity of a body, by unit of mass and temperature. It actually depends on the temperature and its variations are negligible. Table 2.1 presents the values of the density and thermal capacity of various soil components. The isobar soil heat capacity $C_{\rho,soil}$ is expressed by a weighted average of the respective isobar heat capacities of its components, that is to say the usual indices respectively indicating the fractions solid, liquid and gas.

$$C = \frac{dQ}{dT} \quad [J/K] \quad \text{and} \quad C_p = \frac{C_T}{M} \quad [J/Kg.K] \qquad (E\ 1)$$

$C$ Volumetric heat capacity [J/m³.K]

| | | |
|---|---|---|
| $Q$ | Heat content per unit of total volume | [J/m³] |
| $C_p$ | Isobar mass heat capacity | [J/Kg.K] |

Table 2.1: Density and thermal capacity of some soil components

| | p (kg/m³) | Cρ [J/Kg K] |
|---|---|---|
| minerals | 2,65.10³ | 2,10.10³ |
| Organic matter | 1,30. 10³ | 2,47.10³ |
| Water | 1. 10³ | 4,20.10³ |
| air | 1,25.10³ | 1,25.10³ |

$$C_{p,Soil} = [1-(\theta+\theta_a)]C_{\rho s} + \theta C_{\rho W} + \theta_a C_{\rho a} \quad \text{[J/Kg*K]} \qquad \text{(E.2)}$$

With

| | | |
|---|---|---|
| $C_{p,Soil}$ | Isobar soil heat capacity | [J/Kg.K] |
| $C_{\rho W}$ | isobar mass heat capacity of the water fraction | [J/Kg.K] |
| $C_{\rho S}$ | isobar mass heat capacity of the solid fraction | [J/Kg.K] |
| $C_{\rho a}$ | Isobar mass heat capacity of the air | [J/(m³ K)] |
| $\theta_a$ | Voluminal air fraction | [m³/m³] |
| $\theta$ | total Voluminal fraction | [m³/m³] |

**Thermal conductivity**

The soil thermal energy exchanges occur generally simultaneously by conduction and convection, so that the total flux of sensible heat $J_T$ results from the sum of the respective contributions of these two phenomena, that is to say:

$$J_T = J_\lambda + J_S \quad \text{[J/m²s]} \qquad \text{(E.3)}$$

with

| | | |
|---|---|---|
| $J_T$ | total flux of sensible heat | [J/m²s |
| $J_\lambda$ | sensible heat flux transferred by thermal conduction | [W/m²] |
| $J_S$ | sensible heat flux transferred by thermal convection | [W/m²] |

Thermal conduction constitutes a process of heat propagation, gradually, by thermal agitation energy transfer during molecular collisions (Mussy and Soutter). The temperature is an expression of the thermal agitation degree of the consecutive body molecules. When the body temperature is not uniform, i.e. in the presence of heat gradients, then thermal agitation energy transfers occur between the areas with high temperature and the areas with lower temperature. This transfer process ends only when a thermal balance state is established. The sensible heat flux transferred by thermal conduction is thus proportional to a decreasing temperature variation, which is to say according to the Fourier analysis:

$$J_{\lambda} = -\lambda \nabla T \quad [W/m^2] \qquad (E.4)$$

with:

| | | |
|---|---|---|
| $J_{\lambda}$ | sensible heat flux transferred by thermal conduction | [W/m²] |
| λ | Thermal Conductivity | [J/msK] |
| $T$ | Temperature | [K] |

The coefficient of Fourier or thermal conductivity $\lambda$ represents the material resistance to the heat propagation by thermal conduction. The thermal conductivity values of various soil components are shown in Table 2.2. Soil thermal conductivity depends on its composition, its organic and mineral matter content, and also its air content. Thus soil appears to be a bad heat driver when it is dry. Thermal conductivity varies consequently in space and time, in particular according to the water and air content variations.

Table 2.2: Thermal conductivity of some soil components

| | λ [J/msK] |
|---|---|
| Minerals | 2.90 |
| Quartz | 8.80 |
| Organic matter | 0.25 |
| Water | 0.585 |
| Air | 0.023 |

**Thermal conductivity of water repellent soils**

Water repellency affects the soil water distribution and consequently affects some of the thermal properties. That is why water repellency might affect soil thermal properties. Therefore, a study of water-repellency effects on soil thermal properties is needed. There exist only few studies on thermal properties of a water repellent soil.

In a recent study, Bachmann et al. (2001) showed with use of a column experiment that water repellency reduced evaporation.

In addition and in an other paper, Bachmann and al. (2001) make a comparison of the thermal properties of four wettable and four water repellent soils. Thermal conductivity and volumetric heat capacity were determined by heat pulse measurements (Campbell et al. 1991; Welch et al. 1996,;Tarara and Ham. 1997) and water repellency was induced by chemical treatment of wettable soils with dichlorodimethylsilane (C2H6SiCl2). The first model used to estimate soil thermal conductivities for comparison with measured thermal conductivities, was the empirical model of De Vries (1963) and for different ranges of the soil water content, θ (θ = 0.0, 0.0 < θ < θk, and θ > θk , with θk being the critical soil water content and was defined as the equilibrium water content at a pressure potential of -55 kPa).

Figure 2.2 shows the standard effective thermal conductivity model of De Vries (1963) which can predict thermal conductivity of most soils with an negligible error. Our modelled materials have porosity around 0.38. The Johansen model (1975) will be a better prediction for fine soils and dry thermal conductivity (Döll, 1996) but we don't have additional data on particle size distribution.

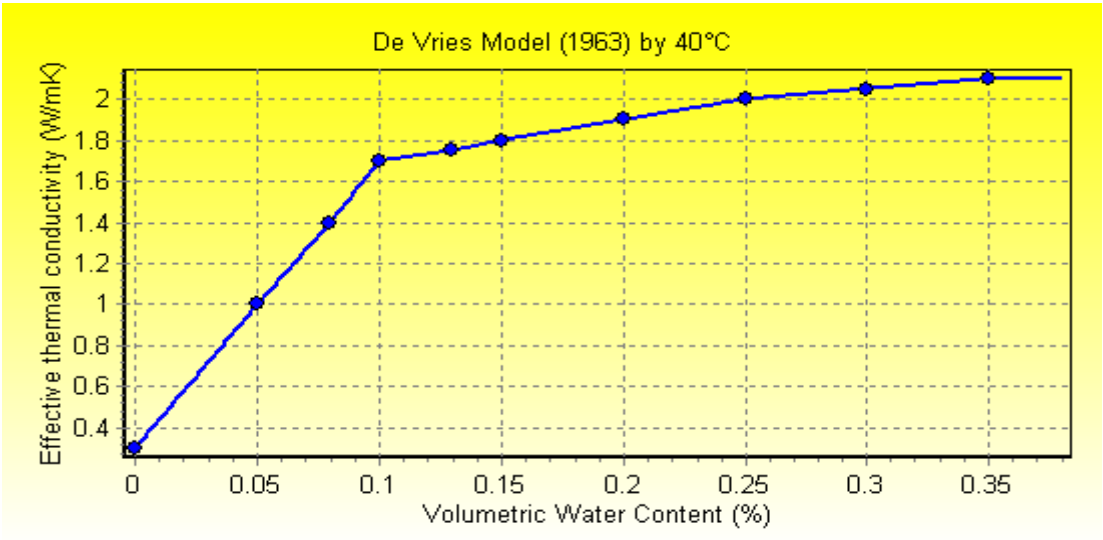


.

Figure 2.2: Thermal conductivity to the De Vries Model (1963) (Döll, 1996)

The second model used, was the model of Campbell (1985). Results show that the thermal conductivity is larger for wettable soils than for corresponding nonwettable soils. A comparison of measured thermal conductivities with two models resulted in considerable deviations between predicted and measured values. The measured conductivities were generally larger than the conductivities predicted by the de Vries model. They find that the prediction of the thermal conductivity matches the measured conductivity data better for the

hydrophobic soils than for wettable soils. It is concluded that soil thermal conductivity decreased as soil hydrophobicity increased, whereas the volumetric heat capacity was not affected by soil wettability.

In (Balland and Arp 2005)Vincent Balland and Paul Arp extend the general applicability of the earlier Johansen (1975) method to model soil thermal conductivity over a wide range of conditions. This new method was then used to re-interpret thermal conductivity data involving wettable and non-wettable soils, in situ field measurements and snow.

Ju and al. (2008) shoed in their study the influences of Dichlorodimethylsilane treatment as hydrophobizing agent on soil hydrophobicity, thermal conductivity and electrical conductivity The results showed that DCDMS reduced the soil thermal conductivity at water contents greater than a critical value compared with wet soil samples.

### 2.2.2. Transport Equations of Heat

**Transfer by Convection**

In the case of thermal convection, the thermal agitation energy transfer is carried out between the molecules located on both sides of a border separating a solid from a moving fluid. Thus transfer is carried out also by fluid mass displacement: which is a problem of fluid mechanics. Interstitial heat density $\delta_T$ expresses heat quantity exchanged during this process. It is thus expressed by the product of its voluminal isobar heat capacity and of the temperature gradient between the solid and the fluid (Musy and Soutter).

When the fluid moves overall under the action of a mechanical force, one speaks about forced convection. The fluid behaviour is then described by the Navier-Stokes law, whose generalized Darcy law is a simplified form, applying in soil context. The significant heat flux transferred by thermal convection is written consequently like the product of the density of interstitial heat and the flux of Darcy.

When there is no forced displacement of the fluid, one speaks then about natural convection. Heat is transferred by the density currents which traverse the fluid, under the effect of the temperature inequalities existing at the interface solid-fluid. The temperature variation thus intervenes in this case doubly, initially by determining the thermal energy transfer of one phase to the other, then by generating movements in the fluid (thermodiffusion).

Natural and forced convections constitute two aspects of the same process and occur generally simultaneously. However, in the heat exchange context occurring in a soil, the main part of the heat transfers by convection is associated with the movements of the liquid and gas phases, so that the natural contribution can be neglected. The characteristic of the

soil heat transfers by convection holds so that they utilize simultaneously two types of fluids: water and air.

**Continuity Equation**

The transitory character of the heat transfers is taken into account by the introduction of the energy conservation principle. In the sensible heat transfers context, this principle states the equality between the thermal energy flux balance, the limits of an infinitesimal soil volume, and the temporal heat variation stored by this volume. The principle of continuity is thus expressed by:

$$\Delta J_T = -\frac{\partial \delta_T}{\partial t} + J_T \qquad \text{(E.5)}$$

$\delta_T$ Heat quantity exchanged during this process

$J_T$ total flux of sensible heat [J/m²s

**Combined Heat and Water Transport**

The general equation describing the soil sensible heat transfers arises from the combination of the dynamic law and the principle of continuity. It can be formulated in various ways.
In the general case of an unsaturated soil, the heat transfer by thermal convection utilizes simultaneously the movements of the liquid and gas phases. Then it is not enough to express flux according to the biphasic flux theory, because it is also necessary to take account of the liquid-vapor transformations through the capillary walls which result in the conversion of thermal energy into latent energy. A more attentive study of this problem reveals that hydrous and thermal flux, in soil, constitute actually interdependent phenomena. Indeed the temperature gradients influence the matrix potential and introduce liquid and gas movements, whereas reciprocally, the moisture space variations, implying hydraulic load modifications, generate fluxes which are carrying heat. These phenomena, occurring simultaneously, are called coupled transfers. The problem resolution thus posed, which is based on physical principles or thermodynamic is not yet realized. If one neglects fluxes from the soil gas phase, the coupled transfers of water and heat can be described by two equations.
The first, expressing water transfers under the combined influence of potential gradient and heat gradient, rises from the partial derivative equation describing liquid fluxes in unsaturated soil to which the thermodiffusion term is added, that is to say:

$$\frac{\partial \theta}{\partial t} = div(K \nabla \psi) + div(D_x \nabla T) + \frac{\partial K}{\partial z} \qquad \text{(E.6)}$$

with

| | | |
|---|---|---|
| $\theta$ | Volumetric Water content | [m³/m³] |
| $D_\lambda$ | Molecular diffusivity of thermodiffusion | [m²/s] |
| $T$ | Temperature | [K] |
| $D$ | Exchange coefficient | [m²/s] |
| K | unsaturated hydraulic conductivity | [m/s] |
| Z | Height or Depth | [cm] |
| $D_\lambda$ | thermal vapor diffusion coefficient | [$m^2$/(sK)] |
| $D$ | isothermal vapor conductivity | [m/s] |

This formulation has the advantage of clearly distinguishing the contributions due to the various forces generating the flux. The second of these equations is the general equation of the heat fluxes to which a latent heat flux term is added due to the vapor flux

$$\rho_w C_{\rho w} \frac{\partial T}{\partial t} = div\ (\lambda \nabla T) - \lambda_1 div\ (D_\lambda \nabla \theta) \qquad \text{(E.7)}$$

Where:

| | | |
|---|---|---|
| $\theta$ | Water content | [m³/m³] |
| $\lambda_i$ | Thermal Conductivity | [J/msK] |
| $\lambda$ | effective thermal conductivity which depend on water content | [W/(m K)] |
| $D_\lambda$ | Molecular diffusivity of thermodiffusion | [m²/s] |
| $T$ | Temperature | [K] |
| $C_{\rho W}$ | isobar mass heat capacity of the water fraction | [J/Kg.K] |
| $\rho$ | density of liquid water | [$kg/m^3$] |

Coupled transfers of water and heat express themselves consequently by the simultaneous application of these two expressions. However, as the two processes which translate these expressions exert an influence each other, it would be necessary, to describe the phenomenon completely, to take account of this interaction.

### *2.3. Radiation and Energy Balance*

The soil temperature translates the mean level of heat stored in soil. Thus the temperature time variations reflect the energy exchanges between soil and the external medium. These exchanges occur primarily between the surface and the atmosphere, in the form of radiative thermal and latent energy. The soil energy analysis relates to the radiative exchanges, whose determines radiative energy net flux arriving at the soil surface, and the sensible and latent heat transfers. The radiative exchanges constitute, from a quantitative point of view, the principal form of energy exchanges between the system soil-vegetation and the atmosphere. Any body of temperature higher than 0°C, emits energy in the form of electromagnetic waves. The intensity of this radiant energy flux and its spectral distribution vary according to the absolute temperature of the emitter, from where the distinction between the solar (high frequency) and terrestrial (low frequency) radiations. Figure 2.3 shows the soil surface energy balance during the day and night and the soil surface radiation budget.

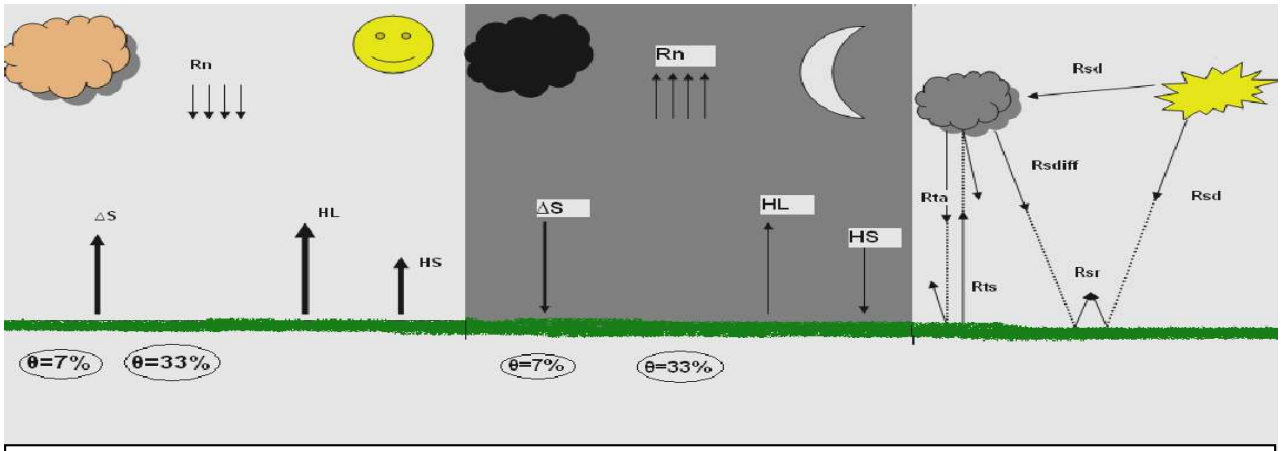


**Energy balance:**

$$R_n + \Delta S + \lambda_E + C = 0$$

**Net radiation:**

$$R_n = (R_{dir} + R_{dif} - R_{ref}) + (R_{atm} - R_{soil})$$

$R_n$ = net radiation

$\Delta S$ = heat flow inside the soil (depend on θ)

$\lambda_E$ = evapotranspiration (latent heat) at the soil surface (HL)

$C$ = sensible heat flow into the atmosphere (HS)

$R_{dir}$ = direct solar radiation

$R_{diff}$ = diffuse solar radiation

$R_{ref}$ = reflected solar radiation

$R_{atm}$ = atmospheric radiation

$R_{soil}$ = soil radiation

Figure 2.3: Soil surface energy balance

### 2.3.1. Radiation and Exchange Processes

**Solar Radiation**

The sun constitutes the independent energy source arriving at the soil surface. The analysis of the solar spectrum shows that it behaves like a black body of a temperature of 6000 °K, which locates its zone of maximum radiative emission in the range wavelength going from 0.3 to 3 micrometers. When a body is subjected to a radiative energy flux, it absorbs a part, reflects another part and transmits the rest of the energy. Its behaviour can thus be described by the three coefficients determining this fractionation and whose sum is equal to 1, namely, transmission, reflexion and absorption coefficients. While crossing the atmosphere, the incident solar radiation is partially attenuated by absorption and scattering in all the directions. These phenomena occur in a different way according to the spectral field. By diffuse reflexion, it is approximately a third of the solar radiation which is returned towards space, this proportion being able to reach 80% when the sky is covered. The total solar radiation, reaching the soil surface, comprises two components: the direct solar radiation transmitted by the atmosphere $R_{dir}$, and the diffuse solar radiation $R_{diff}$, reflected by the atmosphere in the soil direction. The total radiation is partially reflected by the soil according to the nature, the colour, the slope and the ruguosity of its surface. The reflexion coefficient or albedo varies from 0.03 to 0.1 for a water surface, from 0.10 to 0.30 for fields and meadows, from 0.15 to 0.40 for a naked soil and can reach 0.95 for fresh snow. The albedo is much stronger when the direct solar radiation incidence angle is weak. It is thus influenced by the latitude, the season and the moment of the day.

**Terrestrial Radiation and Athmospheric Radiation**

Taking into account an average surface temperature of approximately 300°K, the soil emits a radiation. This long wavelength wavelength in the range of 10µm is in great part absorbed by atmospheric greenhouse gases, particularly by water vapour and carbon dioxide. These gases have an emission spectrum similar to their absorption spectrum, so that the essence of the terrestrial radiation absorbed by the atmosphere is re-emitted, partially in direction of space. Broadly the low frequency radiation is thus negative, except in the presence of a cloud cover which reflects the terrestrial radiation

**Net Radiation**

The assessment of the radiative exchanges on the soil surface is expressed by the net radiation which is thus defined by the sum of the radiations of high and low frequency that is to say the sum of the incidental solar radiations $R_{dir}$ and reflected $R_{diff}$ and of the terrestrial radiations emitted by the soil, $R_{soil}$ reflected by the clouds and emitted by the atmosphere, $R_{atm}$

$$R_n = (R_{dir} + R_{diff}) + (R_{atm} - R_{soil}) \quad \text{(E.8)}$$

The reflected solar radiation is defined by the product of the total radiation $R_g$ and the albedo $\alpha$, so that, by considering that the radiative exchanges at low frequency is negative, the net radiation can be expressed by the relation:

$$R_n = R_g (1 - \alpha) - R_l \quad \text{(E.9)}$$

It appears thus that, during one clear night, that is, absence of solar radiation and of cloud cover likely to reflect the terrestrial radiation an energy loss on the soil level.

### *2.3.2. Soil Atmosphere Interface*

**Sensible Heat Exchange**

The heat transfers between soil and atmosphere occur in the form of sensible heat or latent heat. In the first case, the transfer relates to the thermal energy agitation, whereas in the second this energy was converted into latent energy, the heat transfer being associated to a mass transfer. Many processes contribute to the heat transfers between soil and atmosphere. However the majority of them present a specific character, like the cold or hot water infiltration during precipitations or industrial water rejections. By neglecting these phenomena, to consider only the processes intervening in a continuous way, the sensible and latent heat transfers are limited to the thermal convection process and evapotranspiration respectively. The thermal convection constitutes the principal process of sensible heat transfer between soil and atmosphere. The conveying fluid is then the atmospheric air. In accordance with the principles exposed in the case of soil heat transfers, the sensible heat transfer by thermal convection is carried out simultaneously by natural convection, that is to say by thermodiffusion, and by forced convection, under the effect of a mechanical action.

The sensible heat flux due to the natural convection can be written as follows:

$$C = \rho_a C_{\rho a} D_T \nabla T \quad [W/m^2] \qquad (E.10)$$

Where $\rho_a$ is the air density, $C_{\rho a}$ its isobar mass heat capacity and $D_T$ the molecular diffusivity of thermodiffusion. The sensible heat flux due to the forced convection should be expressed in theory by the product of the interstitial heat density and the air mass flux.

**Latent heat exchange**

The water vaporization implies an energy consumption. The sensible heat converted during this process into latent heat is transferred by vapor mass fluxes. The principles governing the fluxes of the gas phase show that these fluxes can be expressed in a general way by the product of the gradient of concentration, expressed here by its voluminal fraction $v_{vap}$ and of a coefficient of exchange $D_e$, which expresses the diffusive and convective effects characterizing the transfer of the air vapor: The concentration in volume of vapor in the air has a limiting value varying with the temperature, beyond which condensation occurs. It is for this reason preferable to express it by its partial pressure, the relation between saturated vapor pressure and temperature being a physical constant:

$$q_{vap} = -D_e \nabla v_{vap} \quad [m/s] \qquad (E.11)$$

The latent heat flux associated with the stream mass flux is like:

$$\lambda_E = \lambda \rho_a \varepsilon q_{vap} \qquad [N/m^2K] \qquad (E.12)$$

Where $\lambda_E$ is the latent heat of vaporization, $\rho_a$ the air density containing the vapor, $\varepsilon$ the ratio of the vapour molecular weight to that of the air and $\gamma$ the psychometric constant.

**Energy balance formulation**

The energy balance rests on the energy conservation principle. In the energy exchanges context between sun and atmosphere, it states balance between the assessment of the radiative exchanges and the assessment of the heat transfers:

$$R_n = PM + C + \lambda_E + \Delta S \qquad [W/m^2] \qquad (E.13)$$

The net radiation $R_n$ represents, when it is positive, the radiative energy quantity absorbed by the system soil-vegetation and converted into chemical energy and heat, and when it is negative, heat quantity converted into radiative energy. PM represents the part of the radiative energy absorbed by the system and transformed in a chemical energy by the plants metabolism (photosynthesis). It does not exceed a percentage of the net radiation. Consequently it is generally neglected.

$\Delta S$ represents the part of radiative energy converted into heat and stored in the system, after deduction of the sensible latent heat C and latent heat transfers $\lambda_E$. It should be noted that if the energy assessment had been formulated for its surface, the $\Delta S$ term would have been replaced by a term expressing the soil heat transfers by conduction (Jacob, 1999).

## 2.4. *Model Implementation in DELPHIN*

### 2.4.1. Transport Equations

DELPHIN is a numeric simulation interface, which is developed at the Institute of Building Climatology of the Dresden Technical University for the computation of the coupled heat, moisture, air and salt transport in capillary-porous materials. DELPHIN consists of several programs: a Pre-processing program, a Solver and a Post processing program (s. Fig. 2.4) . Data bases for climatic, material and salt data records are attached. The interfaces between the programs are generated in the form of text files, which can be changed by the user.

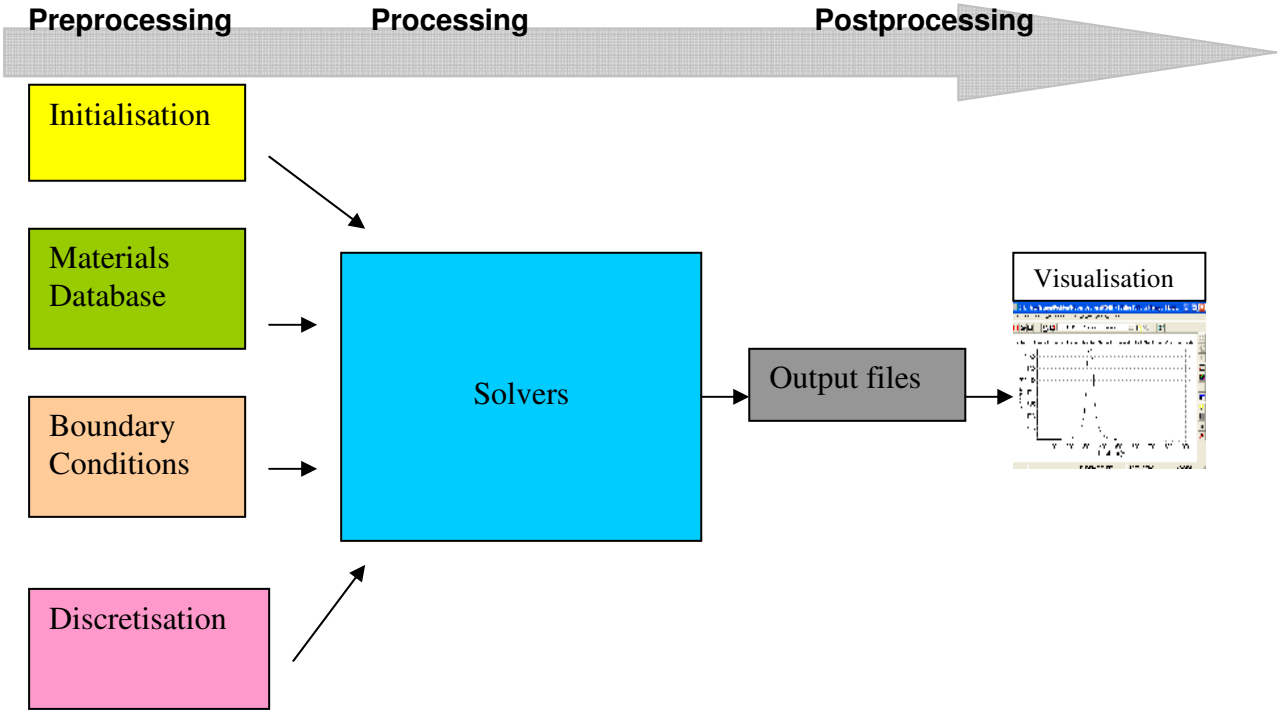


Figure 2.4: Program structure of Delphin with pre and post processing (John Grunewald, 2000)

To implement our physical models for the numerical simulation we used the liquid water pressure gradient model. This implies the liquid water pressure to be the driving potential for advective movement of the liquid phase. In our case, it may not include the moisture mass balance, the air mass transport and the salt advection/diffusion. Only the internal energy balance with gravity in y-direction is taken into account.
The governing balance equation is:

$$S_{41}\frac{\partial \theta_l}{\partial t}+S_{42}\frac{\partial P_g}{\partial t}+S_{43}\frac{\partial C_s}{\partial t}+S_{44}\frac{\partial T}{\partial t}=-\frac{\partial}{\partial x_k}[\rho_l\mu_l\nu_k^{m_l}\theta_l+(\rho_v\mu_v+\rho_a\mu_a)\nu_k^{m_g}\theta_g]$$

$$-\frac{\partial}{\partial x}[(h_v-h_a)\,j_{j,diff}^{m_v}\,\theta_g] \quad \text{(E.14)}$$

With:

$$S_{41}=\rho_l\mu_l+\nu_v\left(\frac{\theta_g}{R_vT}\rho_{vs}\frac{\partial\varphi}{\partial\theta_l}-\rho_v\right)-\mu_a\left(\frac{\theta_g}{R_aT}P_{vs}\frac{\partial\varphi}{\partial\theta_l}+\rho_a\right) \quad \text{(E.15)}$$

$$S_{42}=\mu_a\frac{\theta_g}{R_aT} \quad \text{(E.16)}$$

$$S_{43} = (\rho_p \mu_p - \rho_v \mu_v - \rho_a \mu_a) \frac{\partial \theta_p}{\partial C_s} + \rho_l \theta_l \frac{\partial \mu_l}{\partial C_s} + \mu_l \theta_l \frac{\partial \varphi_1}{\partial C_s} + (\mu_v \frac{\theta_g}{R_v T} - \mu_a \frac{\theta_g}{R_a T}) P_{vs} \frac{\partial \varphi}{\partial C_s} \quad \text{(E.17)}$$

$$S_{44} = \rho_m \frac{\partial \mu_m}{\partial T} + \rho_l \theta_l \frac{\partial \mu_l}{\partial T} + \rho_p \theta_p \frac{\partial \mu_p}{\partial T} + (\rho_v \frac{\partial \mu_v}{\partial T} + \rho_a \frac{\partial \mu_a}{\partial T}) \theta_g + \mu_l \theta_l \frac{\partial \rho_l}{\partial T})$$

$$+ ((\rho_p \mu_p - \rho_v \mu_v - \rho_a \mu_a) \frac{\partial \theta_p}{\partial C_s} + \mu_v \frac{\theta_g}{R_v T} (P_{vs} \frac{\partial \varphi}{\partial} + \varphi \frac{dP_{vs}}{dT} - \frac{P_v}{T})$$

$$- \mu_a \frac{\theta_g}{R_a T} (P_{vs} \frac{\partial \varphi}{\partial} + \varphi \frac{dP_{vs}}{dT} + \frac{P_a}{T}) \quad \text{(E.18)}$$

### 2.4.2. Model Geometry and Soil Physical Properties

Figure 2.5 and 2.6 shows the spatial geometry of our models. They reproduce a vertical sandy soil profile of 1 meter width and 1 meter depth and without vegetation cover. In our first model concept, the wettable area is 4 cm wide and 40 cm deep. We took two classes of sandy soil which have the same physical properties but the thermal conductivity coefficients are different (Trinks, Schulgarten, 2008). In Table 3, basic material parameters of our modelled materials are given. In the second model concept the difference lies in the fact that the wet area is 40 cm wide and 40 cm deep. These models reproduce respectively the field investigations in Berlin-Tiergarten and Berlin-Buch.

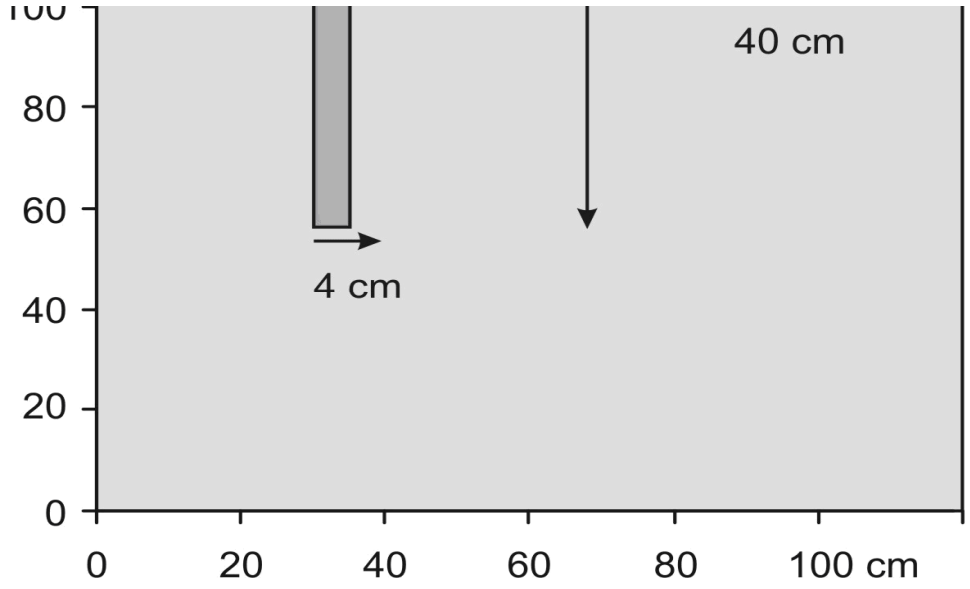


Figure 2.5: Scenario I where the wet area is 4 cm wide

Wet soil with $\lambda_2$ as thermal conductivity

Dry soil with $\lambda_1$ as thermal conductivity

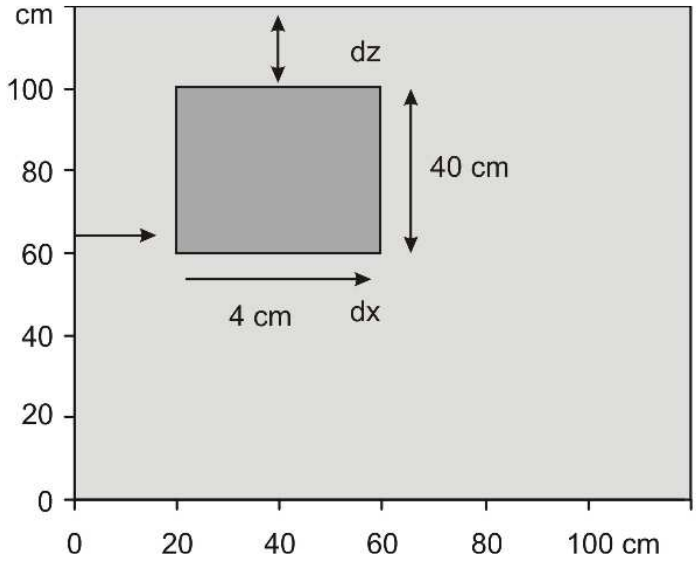


Figure 2.6: Scenario II where the wet area is 40 cm large

Table 2.3: Basic soil material parameters

| Soil | $\theta_{por}$ (vol%) | $\theta_{eff}$ (vol%) | $\theta_{cap}$ (vol%) | $\rho$ (kg/m³) | C (j/kgK) | $\lambda$ (dry) (w/mK) |
|---|---|---|---|---|---|---|
| Dry soil | 38 | 37.9 | 37.7 | 1664 | 850 | 0.3 |
| Wet soil | 38 | 37.9 | 37.7 | 1664 | 850 | 0.3 |
| Air 50mm | 100 | 0.9999 | 99.9 | 1.29 | 1000 | 0.3 |

Figure 2.7 shows the thermal vapour diffusion coefficient of our modelled soil as a function of gravimetric water content. But in our simulation we don't use it because we take only into account heat and energie transfers. Nevertheless to determine well our soil characteristics the Figure 2.8 gives us information about the soil hydraulic conductivity.

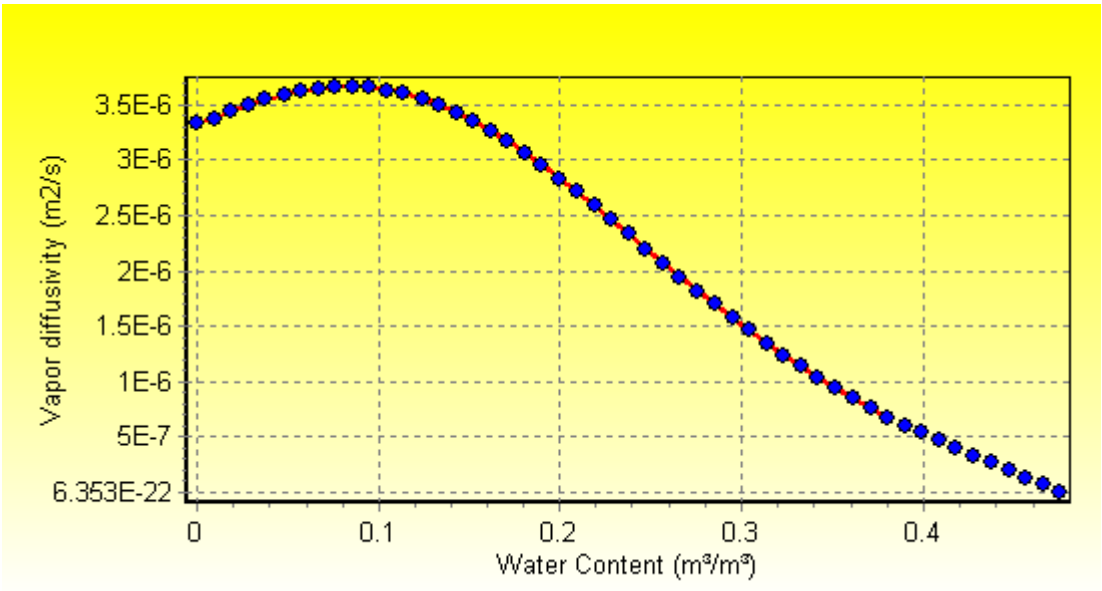


Figure 2.7: Vapour diffusivity of the soil

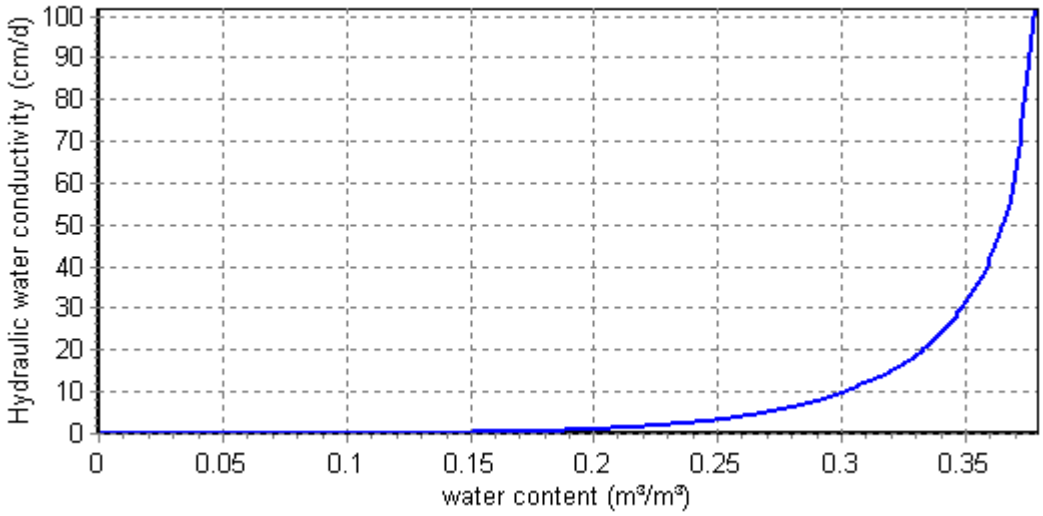


Figure 2.8: Hydraulic conductivity of the 2 sandy soils from Berlin-Tiergarten (Trinks, 2008)

### 2.4.3. Initial and Boundary Conditions

The initial and boundary conditions play a big role in the determination of the soil surface temperature. Moreover climatic parameters vary considerably in space and in time and they intervene directly in the calculation of this soil surface temperature.

Natural, climatic site conditions (e.g. temperature, relative humidity, rain, wind velocity, wind direction, short and long-wave radiation) are present in climatic data sets. These conditions are to be assigned to the soil surface necessarily over a climatic boundary condition. Because the surface temperature strongly depends on the radiation and evaporation, that's

why we chose a sunny period of the year where the sky is cloudless. Figure 2.9 shows the temperature data during our simulation period. It starts at 30 august and runs for 8 days.
For our simulation, heat conduction, long wave radiation, short wave radiation and vapour diffusion are imposed at the soil surface as boundary conditions. The climatic conditions required, is of North Germany.
An initial soil temperature of 15 ° C is also applied. The dry soil had initially 5 volume percent as water content and 10 volume percent for the wet soil.

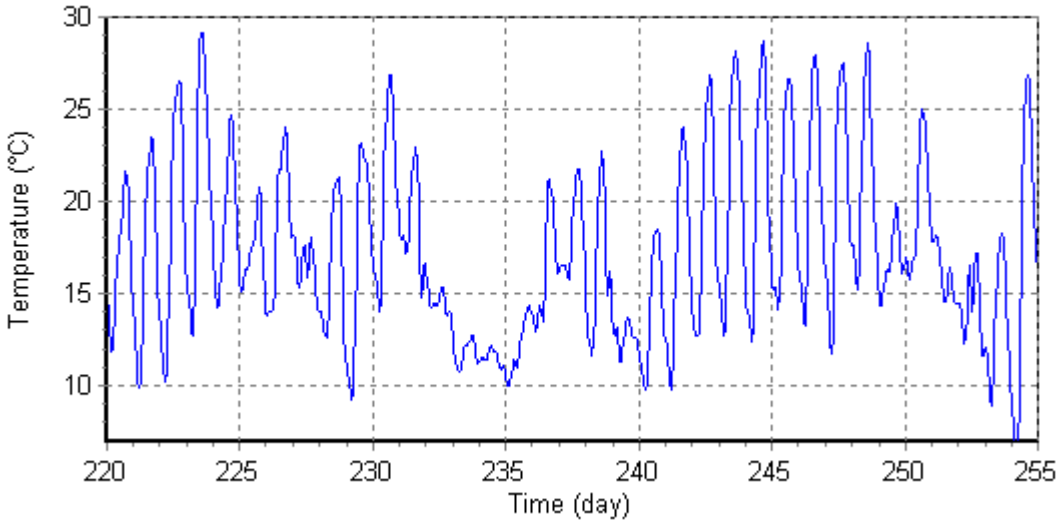


Figure 2.9: North Germany temperature between day 220 and day 255 (climatic database, Delphin 4 version 2006)

## 2.5. Results of the Numerical Studies

The soil surface temperature fluctuates under the influence of the air temperature, and the solar radiation. Figure 2.10 shows a comparison of the soil surface temperature between wet soils with $\theta$=0.10 Vol% and dry soils with $\theta$=0.05 Vol% according to the local position at the surface during the day and during the night under scenario II. The dry soil surface temperature remains almost spatially constant and reaches a maximum of 26,70℃ during the day and a minimum of 12,18℃ before sunset. Above the wet zone a stable temperature exits around 12,51℃ during the night and about 26,01℃ during the day. We have a transition zone arround 10 cm where the soil surface temperature fluctuates. During the day the dry soil surface temperature remains higher than the wet soil surface temperature and in the night we observe the opposite phenomena, because during the night the solar radiation

and evaporation effects are negligible. And we have an energy loss on the surface level due to terrestrial radiation.

The Figures 2.10 and 2.11 show the daily (between sunrise and sundown) soil surface temperature variation between wet soils with θ=0.10 Vol% and dry soils with θ=0.05 Vol% according to the local position at the surface under scenario I and scenario II respectively. Till 25 cm the dry soil surface temperature remains constant of 25,58°C in Scenario I and 26,70°C in Scenario II. From 25cm till in the middle of the wet soils in particular 32 cm and 50 cm in Scenario I and Scenario II respectively, the soil surface temperature decreases till 25,08°C in Scenario I and till 26,01°C in Scenario II. It remains constant till 60 cm in Scenario II. From 32 cm till 42 cm in Scenario I and from 60 cm till 82 cm in Scenario II, the soil surface temperature grows till 25,58°C and 26,70°C in Scenario I and in Scenario II respectively. Below it remains unchanged. During the day the soil surface temperature reached his minimum value in the middle of the wet soils, and at the night the soil surface temperature reached its maximum value. The temperature falls at the entry of the wet area during the day is due to the soil heat transfer effects. The differences of the soil surface temperature between the wetter and dryer parts of the soil is 0,50°C in Scenario I and 0,71°C in Scenario II. That's why a soil with low thermal conductivity has a temperature superior to the soil with high thermal conductivity during the day. The physical parameters implied in the surface temperature calculation being variable in time and in space, it was then necessary to make a sensitivity study. Thus, the initial water content variation between wettable and dry area, or the covering depth of this wettable zone, and finally the vegetation cover can influence this surface temperature.

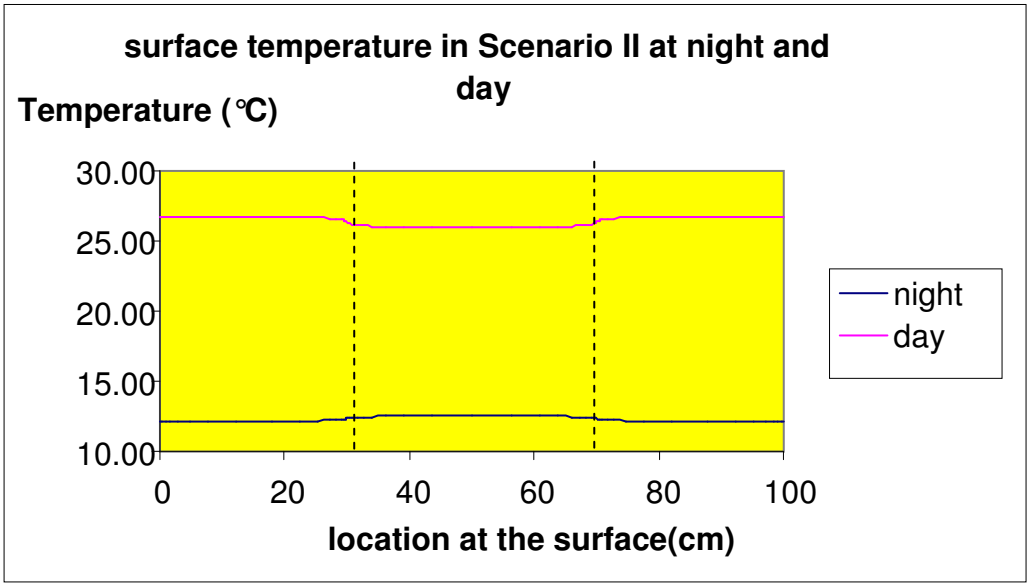


Figure 2.10: Surface temperature according to the positions in Scenario II at night and at day

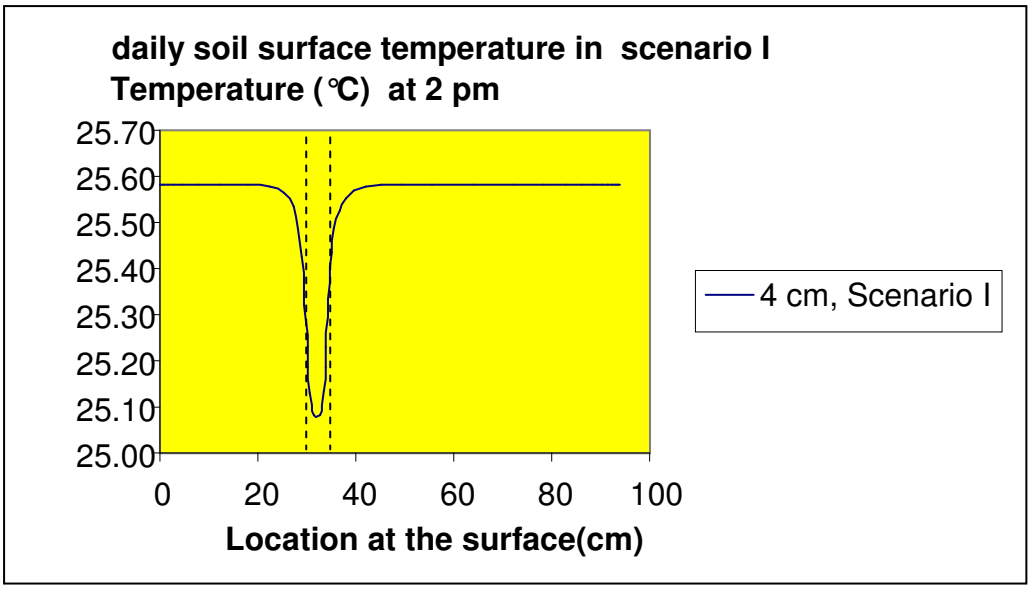


Figure 2.11: Surface temperature according to the positions in Scenario I where the temperature difference between wet and dry zones reach his maximum

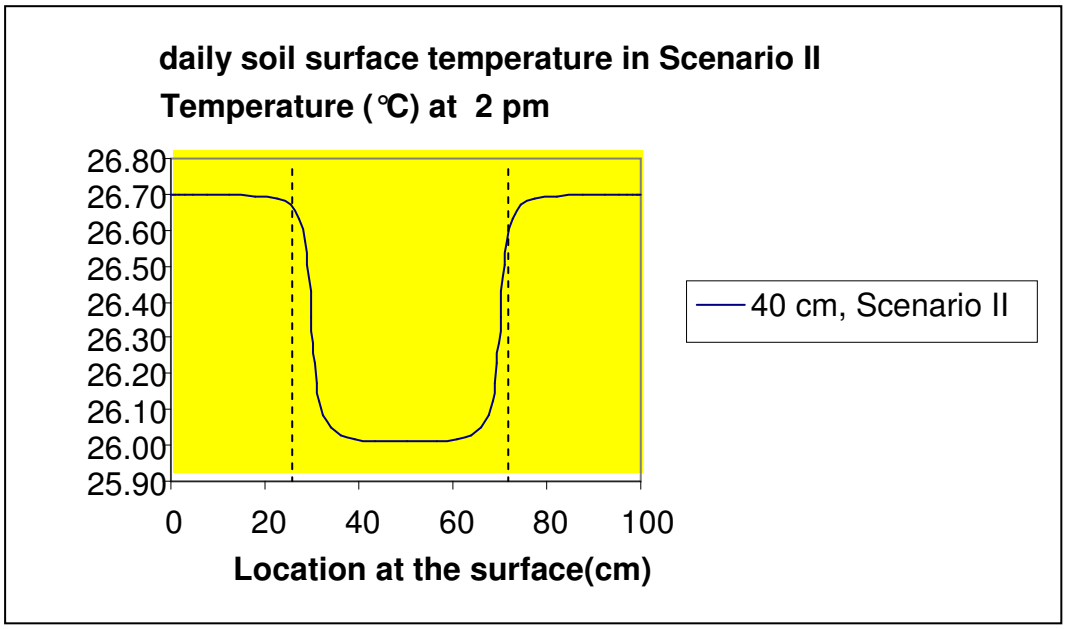


Figure 2.12: Surface temperature according to the positions in Scenario II where the temperature difference between wet and dry zones reach his maximum

Because in most of water repellent soils, wettable soils next to dry soils like in the Figure 2.1 are found deep in the soil and not at the surface. These can generate a temperature gradients which can influence the surface temperature. To which depth limits these wettable zones can be buried so that they exert an influence on the surface temperature?

The Figure 2.13 analysis shows that if the wettable soil starts at the surface, then the daily surface temperature fluctuates with a temperature difference between wet and dry soils of about 0,68°C, and this wave amplitude decreases till 0.10°C if the wet soil is starting from 5 cm depth. When the wet soil starts from 10 cm depth, we notice a uniform soil surface temperature. We conclude that with increasing spots and sizes of wetable zones the soil surface temperature differences (between wet and dry zones) become small. Consequently its influence on the soil surface temperature decreases with its size.

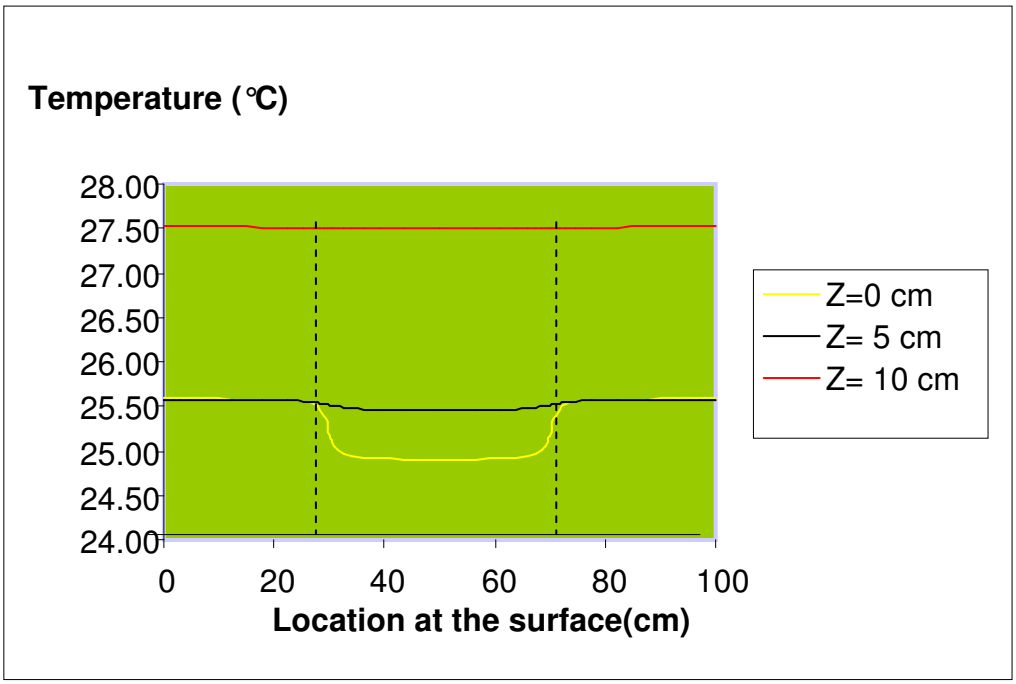


Figure 2.13: Surface temperature space variations in Scenario II according the wetable area covering depth

For the initial water content variation sensitivity study, we simulated our models for various values of water content. At first we simulated a variation of 2,5 volume % (dry soil: 5% and wettable soil 7,5%) then we increased this initial water content difference to 15 volume % for that we calculated the maximum between the differences in temperature of wet and dry soils.The analysis of Figure 2.16 shows that the maximum temperature difference between wet and dry zones varies with the initial water content difference. If the wet soil starts at the soil surface then this maximum is 0,34°C in scenario I and 1,02°C in scenario II. These values decreases according this wet soil covering depth and reached 0,16°C for scenario I and 0,45°C for scenario II at 5 cm covering depth, for finally cancelling themselves in scenario I and reach 0,18°C at 10 cm wet soil covering depth. The more the water content difference is great, the more the soil surface temperature difference between wet and dry zones is large. We can notice also that for 10 cm covering depth of the wet soil the maximum

temperature difference between wet and dry soil is negligible for an initial water content difference of 2.5 volume % in opposite of the model with initial water content difference of 15%.

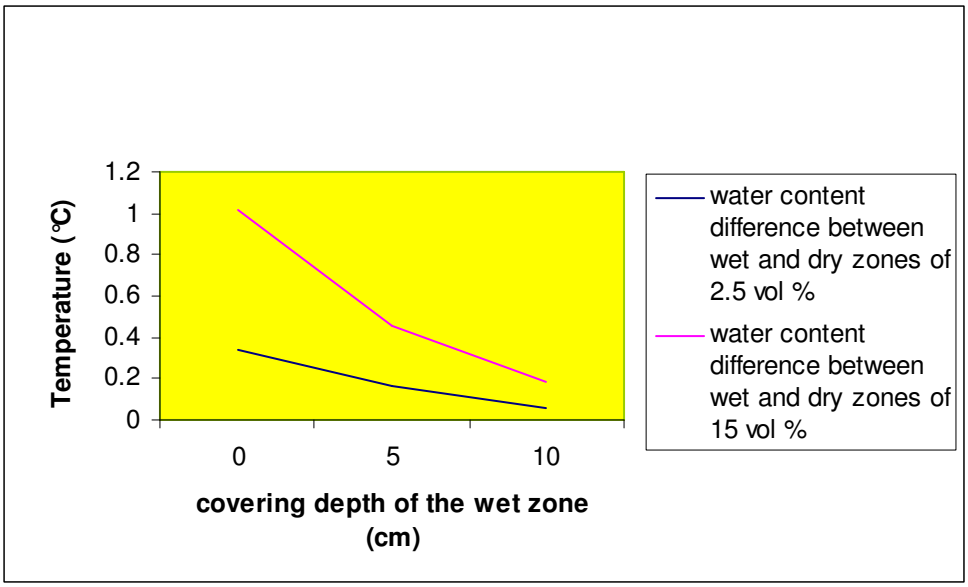


Figure 2.14: Maximum temperature difference of the daily surface temperature between wet and dry zones in Scenario II

## *2.6. Conclusions*

The numerical scenarious lead to the following conclusions:

- The size of the wettable area as well as the initial water content difference between wet and dry soils did not have a large influence on the soil surface temperature.
- The wet soil covering depth deadens gradually the soil surface temperature wave in depth, that is to say it reduces the maximum between the differences in temperature of wet and dry soils.. Thus below 10 cm, this influence was almost negligible. These covering depths of the wet soils and the vegetationcover, influence particularly the heat exchange effectiveness with the air.

The developed model integrates the majority of the thermal phenomena intervening in the exchange between the air and the soil, except for the soil water infiltration. This soil thermal model takes into account of many parameters and is adapted to any type of real situation. On the other hand, its calibration was not completely finalized yet.

## 3. Detecting Water Repellency using Thermography

### *3.1. Introduction*

Information resulting from teledetection was the subject of several studies relating to the characterization of agricultural surfaces. In this comprehensive view, the thermal answer of the soil under various hydrous and weather conditions is a way of research strongly exploited for the follow-up of the irrigation and the prevention of the dryness conditions. Several studies connected the heat balance at the soil surface to the physiological processes which are the evapotranspiration and photosynthesis (Wiegand et al, 1983; Moran et al, 1994; Yuan et al, 2004). Among the methods used to estimate and measure this assessment, the thermal infrared teledetection has the advantage of the speed and the facility of acquisition. This led to the development of several indicators of hydrous stresses based on the relation which exists between the temperature, the optical properties of the plants and their hydrous state. The use of these indicators in precision agriculture encounters several limits. The majority of the indicators were developed by using satellite and airborne measurements to establish diagnoses with the regional scales. However, the environmental factors which condition transpiration on the plant level as well as the structure of the vegetation cover require more precise measurements.

The theoretical bases and the weaknesses raised in the presentation of the problems justify the development of a water repellency indicator which is accessible by thermal infrared teledetection, and which constitutes a diagnostic tool. Thermography measurements with an infrared camera associated with the optical imagery could meet this need.

**Study Targets**

The aims of this study is to test whether infrared thermography can be used to detect water repellency structures of the soil surface. This should be possible because of the following assumptions:

- In a water repellent soil, dry soil can exist next to zones of wet soil. This variation of initial water content between dry and wet zones can cause differences in the total amount of soil heat to the soil surface.
- At night(sundown), the evapotranspiration effect on surface temperature is negligible.
- The absence of the direct solar radiation during the night leads to a dominant influence of the soil heat transport to the soil surface.

## 3.2. The Temperature of Vegetation as Indicator of Water Repellency

Several methods were used to estimate the vegetation temperature, however the use of the thermal infrared teledetection is that what seems to be a promising way. It has the advantage of the speed and the facility of acquisition.

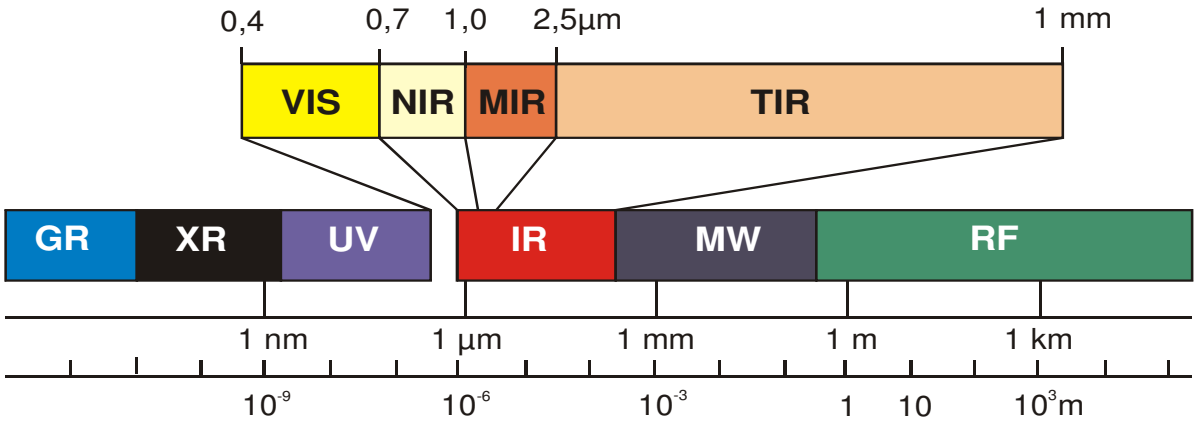


GR: Gamma Rays
XR: X Rays
UV: Ultraviolet
VIS: Visible
MIR: Midinfrared
IR : Infrared
NIR : Near Infrared
TIR : thermal Infrared
MW : Microwaves
RF : Radio Frequency

Figure 3.1: Electromagnetic spectrum (Serge Olivier Kotchi, 2004)

### 3.2.1. Physical Principles

**Planck Law**

The Planck law (Max Planck, 1858 - 1947) described the radiation ermitted by a black body, according to the wavelength and the temperature. It permits to measure temperatures by radiation. When a body temperature increases, it emits a radiation in the form of electromagnetic radiation. The thermal infrared sensors measure this radiation emitted in the infrared band (IR, 0.7 with 100µm) of the electromagnetic spectrum and connect it at body temperature by the Stefan-Boltzmann law and the Planck law (Gaussorgues, 1999).

$$W_{\lambda b} = \frac{2\Pi hc^{2}}{\lambda^{5}(e^{\frac{hc}{\lambda kT}} - 1)} \quad [3.1]$$

| | | |
|---|---|---|
| $c$ | Speed of light: $3x10^{8}$ | [$m.s^{-1}$] |
| $W_{\lambda b}$ | Radiation of a black body to the wavelength | [$Wm^{-2}\mu m^{-1}$] |
| $\lambda$ | Wavelength | [m] |
| $h$ | Planck's constant : $6.63x10^{-34}$ | [Js] |
| $k$ | Boltzmann's constant : $1.38x10^{-23}$ | [$J.K^{-1}$] |
| $T$ | Temperature | [K] |

**Displacement Law of Wien**

The displacement law of Wien is obtained by the derivation of the Planck law. It gives the maximum wavelength corresponding to the maximum of radiation of a black body according to its temperature. The displacement law of Wien thus explains displacement towards the short wavelengths emission of the increasingly hot bodies.

$$\lambda_{\max} = \frac{2897.9}{T} \quad [3.2]$$

| | | |
|---|---|---|
| $\lambda_{\max}$ | Wavelength corresponding to the maximum of radiation | [m] |
| $T$ | Temperature | [K] |

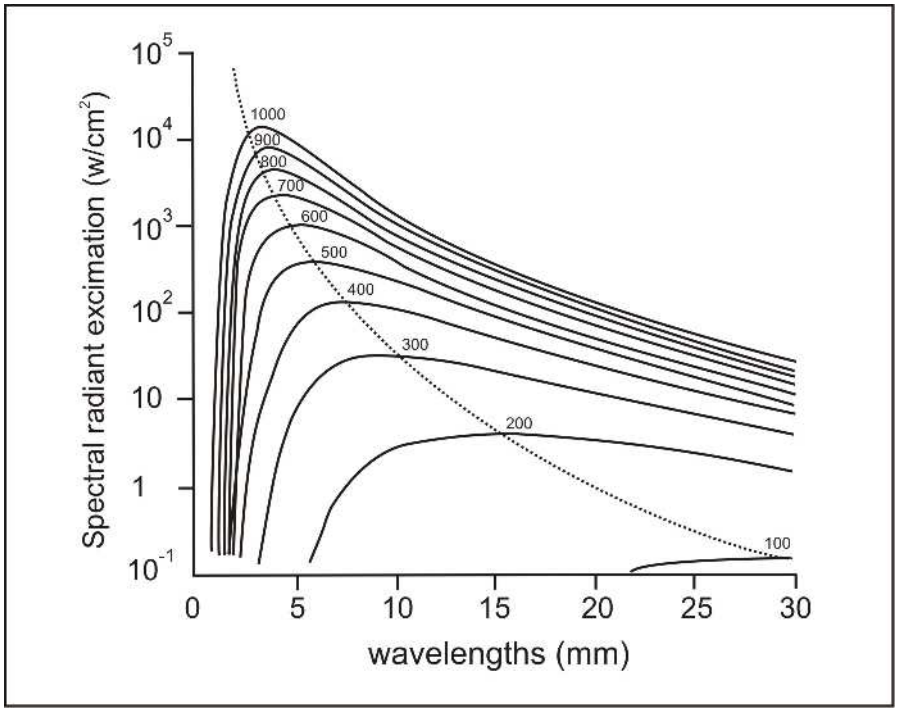


Figure 3.2: Displacement of the emission maximum towards the short wavelengths of the increasingly hot body (Serge Olivier Kotchi, 2004)

**Stefan-Boltzmann Law**

The law of Stefan-Boltzmann is the integration on the whole wavelengths of the Planck law. It expresses the total energy ($M_b$) irradiated by a black body for a temperature T given. It also shows that the body emission is strongly dependent on the value of its high temperature to power 4.

$$M_b = \int_0^{+\infty} \frac{2\Pi hc^2}{\lambda^5 (e^{\frac{hc}{\lambda kT}} - 1)} d\lambda = \sigma T^4 \qquad [3.3]$$

| | | |
|---|---|---|
| $\lambda$ | Wavelength | [m] |
| $M_b$ | Black body exitance | [$Wm^{-2}$] |
| $\sigma$ | stefan-Boltzmann constant 5,67032.$10^{-8}$ | [$Wm^{-2}K^{-4}$] |
| $c$ | Speed of light: 3x$10^{8}$ | [$m.s^{-1}$] |
| $h$ | Planck's constant : 6.63x$10^{-34}$ | [Js] |
| $k$ | Boltzmann's constant : 1.38x$10^{-23}$ | [$J.K^{-1}$] |
| $T$ | Temperature | [K] |

**The Emissivity and the Radiation of Natural Surfaces**

Contrary to a black body, natural surfaces are not perfect radiators. They are called "body gray" in the literature. For these bodies, the Stefan-Boltzmann law integrates the emissivity concept. Emissivity measures the radiation effectiveness of a natural body compared to a black body. It varies according to the wavelength and lies between 0 and 1. In the thermal infrared, certain surfaces (water, basalt, vegetation) behave like black bodies and their emissivity approach 1.

$$M = \varepsilon \sigma T^4 \qquad [3.4]$$

| | | |
|---|---|---|
| M | body exitance | [$Wm^{-2}$] |
| $\sigma$ | stefan-Boltzmann constant 5,67032.$10^{-8}$ | [$Wm^{-2}K^{-4}$] |
| $T$ | Temperature | [K] |
| $\varepsilon$ | Emissivity | |

### *3.2.2. Canopy Temperature Variability (CTV) Spectral IRT Index to Detect Water Repellency by a Critical Water Content Threshold*

For a better comprehension of radiometer measurement, it is necessary to clarify the expressions: vegetation cover temperature (Tc), surface temperature (Ts) and soil temperature (To). The cover temperature (Tc, Canopy temperature) was defined like the radiometric temperature measured in the thermal infrared (IRT) and for which the vegetation is dominant in the sight field of the sensor, the soil effect being tiny (Moran, 2000). Kustas et al (1990) defined Ts like a Tc function and To.

$$T_s^4 = f_c T_c^4 + (1 - f_c) T_0^4 \qquad [4.5]$$

| | | |
|---|---|---|
| $f_c$ | Vegetationcover fraction | |
| $T_s$ | Surface temperature | [°C] |
| $T_c$ | Vegetation cover temperature | [°C] |
| $T_0$ | Soil temperature | [°C] |

When the soil is completely covered by the vegetation, then Ts = Tc.
The majority of natural surfaces, just like the plants, have their maximum of emission in the IRT.

The surface temperature of vegetation covers led to the development of several indicators of hydrous stress. The theoretical base of these indicators rests on the relation existing between the plants temperature and their hydrous state
Since the soil is not homogeneous inside a field, the water lack will involve a cover temperature spatial variability. The cover temperature spatial variability inside a piece is thus used like a hydrous stress indicator inside this piece (Berliner et al, 1984; Bariou et al, 1985a; Penuelas et al, 1992; Moran, 2000). The CTV is the standard deviation of the average cover temperature. When the CTV value exceeds 0,7, cover is considered in hydrous stress. One of the advantages of CTV index is that it does not require the air temperature measurement, and can be calculated with Tc values acquired starting from airborne sensors IRT without atmospheric correction (Moran, 2000). The environmental factors constituting a brake with these first above mentioned indices, more complex models, combining the surface temperature measurement by sensors IRT and the evapotranspiration physics, were elaborated. Among those, let us quote Crop Water Stress Index (Wiegand et al, 1983) and the Water Deficit Index (WDI, (Moran et al, 1994)).

$$CTV = \sigma(T_c) \quad [4.6]$$

| | | |
|---|---|---|
| $T_c$ | Vegetationcover temperature | [°C] |
| $\sigma$ | Standard deviation | |

### *3.3. Materials and Methods*

#### *3.3.1. Study Site: Berlin Tiergarten*

The study site is a large park in the centre of Berlin (52°30´45" N, 13°21´13"). Originally conceived as a hunting ground for Prussian Kings, the Tiergarten was transformed into a romantic landscape garden in the early 18th century. The annual precipitation and mean air temperature of the site are between 555 and 570mm, and 10.5°C respectively.

The site presently is dominated by grassland, Bush planting and herb Corridors. The soil is classified as a Terric Anthrosol with medium sized-sand, fine sand and medium-sized loamy sand being the textural fraction. Table 3.1 shows selected physical and chemical properties of the soil.

The soil is composed up till 15 cm depth of a medium humus content and a poor carbonate content of a black upper soil horizon with polyhedron structure over a weakly gravel of loamy sand from building debris.

From 15 to 60 cm we have a weakly humus content and carbonate content of a dark grizzly brown horizon with single grain and polyhedron structure over a strongly gravel sandy clay from building debris with a mortars portion. From 60 to 80 cm we found a medium humus content of a very dark brown fossil upper soil horizon with single and polyhedron structure over a high cryoturbation loamy sand. Under 80cm we found a medium humus content of a brown to dark brown horizon over a high cryoturbation loamy sand.

The organic matter content of the topsoil is 2,2%(g/g), below a depth of 15 cm the organic matter content is approximately 0,88%(g/g) while further increasing to 1,87%(g/g) below 60 cm. The groundwater table was approximately 210 cm below the soil surface.

Table 3.1: Some soil information on the Tiergarten soil

| Depth | Horizon | pH | C_org | Munsell |
|---|---|---|---|---|
| Cm | | $H_2O$ | (% g/g) | |
| Ah | | 7,4 | 2,21 | 10YR2/1 |
| 15-60 | jM | 8,6 | 0,88 | 10YR4/2-3/2 |
| 60-80 | fAh | 7,4 | 1,87 | 10YR2/2 |
| 80-125 | Ah-Bv | 7,8 | n.b | 10YR4/3 |
| 125-200 | rGr | | | 10YR7/2 |
| >200 | Gr | … | … | 2.5Y5/3 |

### *3.3.2. Tracer Experiment and Soil Sampling*

We applied an impulse of 30mm water after we sprayed 2mm Brilliant Blue tracer with a pesticide hand sprayer. We used a similar photographic setup, as described in Nehls et al., (2006). The camera was fixed at a 2-meter-high tripod. Horizontal cross sections parallel to the soil surface were prepared at the depths 4cm, 10cm, 20cm and 30cm. For each horizontal cross section photographs were tacked together with Kodak colour and grey scales paperboard in the picture. In order to estimate the brilliant Blue concentrations in the pictures from the colour spectra the specimen positions were marked and each cross section was noted on different photographs and then 108 soil samples were collected at depths 4cm, 10cm, 20cm and 30cm. The sampling positions were distributed across a plot of 90cm by 60 cm with a high resolution in a grid of 8cm by 6cm. These field samples allows us to determine the spatial distribution of the water repellency and the gravimetric water content. Soil surface water content were also measured by using TDR along a transect of 10cm by 10cm.

To estimate Brilliant Blue concentrations in the images from the color spectra, a calibration against measured dye concentrations is needed. A thin layer of approximately 12 to 15 g of soil was scraped from homogeneously stained and unstained areas with different dye intensities. In total, 80 samples were taken from the plots. The sampling locations were marked and each cross section was recorded on separate photographs.

### *3.3.3. Thermal Camera*

Infrared thermography is a teledetection process which calls upon the electromagnetic radiation laws to convert the thermal infrared radiation of any objects surface, in visible images. The fact that the radiation is a function of the object surface temperature, allows to calculate this temperature. The images thus obtained make it possible to visualize differences in temperature which differently would be remained unperceived. Contrary to the traditional cameras which collect only wavelengths ranging between 0.4 and 0.7 micrometers, the infrared camera works in the band ranging between 2 and 15 micrometers. This property of thermal imagery associated with infrared thermography gave place to many applications.

The first military apparatuses for the visualization of the thermal radiation appear in the United States, at the end of the Fifties. Nearly ten years later, the first industrial measurement asset were designed and produced by Swedish company AGA Infrared Systems. These apparatuses were immediately adopted by the medical world, especially with the end of detection and follow-up of cancerous tumours. Today infrared thermography knows many applications in petrochemistry and electricity, construction trades, for the escapes detection, the control of oil pollution, fires monitoring, the weather, geographical or medical analysis. The radiation measured by the cameras is not only dependent on the object temperature, it is also function of emissivity. The object radiation is influenced by reflected radiation and the interaction with the atmosphere. The interaction with the atmosphere is at three levels:

Absorption and the diffusion by the atmospheric particles cause an attenuation of the flow transmitted by energy dissipation

The air movements involve local temperature variations, pressure and moisture, causing fluctuations of the atmosphere refraction index. This atmospheric turbulence deforms the wave front and inflects the energy rays trajectory.

We used a thermal scanner camera with high spatial dissolution and accuracy. Varioscan high resolution is the world's first portable thermographic camera from the German manufacturer JENOPTIK for wavelength covering 2-5 µm (system 3022) 8-12 µm (system 3021, system 3021-Str.). The detector signal is strengthened with a resolution of 8 colours Bit (256, digitized with 16 bits and visibly made). The temperature resolution is ±0,03°C. The measuring temperature range is between -40°C and +1.200°C, the application temperature range is from -10°C to 40°C.

For this experiment in Tiergarten, we took a Plot of 90 cm by 60 cm. The Thermal camera was attached to a tripod with a locally fixed position in the centre of the plot. The distance

between the camera and the topsoil was 1,5 meters. The photographic records were taken all 30 second on Monday 12/06/2006 of 14 o'clock to 22 o'clock 30 and on Tuesday 13/06/2006 of 6 o'clock 45 to 22 o'clock 30 and on Wednesday of 6 o'clock 45 to clock 12 o'clock.

Figure 3.4: Varioscan thermal cameras

### *3.3.4. Meteorological Measurements*

**Energy balance**

With the radiation balance measurement, the short-wave and long-wave components of the energy balance are within a range of 0,3 - 60 µm. In this measure the sun - and sky radiation, artificial light sources radiation and surface reflection radiation are included. With this equipment we can measure also the wind velocity, wind direction, acoustic temperature, air temperature, relative humidity.

**Air temperature and air humidity**

The psychrometer is an instrument formed by the association of two thermometers of which one is wet and the other is dry. If the air moisture is saturated, the two thermometers indicate the same temperature, but in dry weather, the wet-bulb thermometer shows a lower temperature

Before reading, a small integrated ventilator is engaged in order to air the two thermometers. It is then possible to work out psychrometric equations and to deduce the air water content by interpolation with a saturation curve. The psychometer equation is written:

$$e_a = e(T_H) - \gamma(T_a - T_H) \qquad [4.7]$$

| | | |
|---|---|---|
| Temperature of the wet thermometer | | [K] |
| $T_a$ | Temperature of the dry thermometer | [K] |
| $e(T_H)$ | Vapor tension saturated at the temperature with the wet thermometer | [K] |
| $\gamma$ | Psychometric coefficient:=66 | [Pa/K] |

This equation is not rigorous because it does not hold account of the ventilation which however influences the psychrometric coefficient. There are three great types of psychrometers: all are graduated and information is obtained by direct reading:

- with natural ventilation (under shelter)
- psychrometers slings
- psychrometers with aspiration

**Wind Speed and Direction**

The wind direction is obtained with a vane coupled to an anemometer which gives its speed. The anemometer is a winch of three cups actuating a magnet which induces by rotation a current proportional to the wind speed. This one is related to the "roughness" of the soil surface and the vegetation. This speed increases with altitude in logarithmic manner and beyond a "layer-limit", one reaches the free atmosphere. There exists in fact various types of anemometers:

- With winch or propeller. It is the mostly used type
- Other types: static, thermal and sonic anemometers. They function on radically different principles but provide the same information

### *3.3.5. TDR -Measurements*

A D-LOG/mts (EASY TEST Ldt., Lublin, Poland) device was used. It operates using a needle pulse type generated electromagnetic waves with 300 ps rise time, and the electromagnetic radiation has a frequency range from 30 MHz up to 1.6 GHz (Malicki and Skierucha, 1989).
The 2 sensors measure the soil volumetric water content. Used in the beginning to test electric circuit cables, the TDR method developed quickly since it is of a relatively simple employment and allows a volumetric water content measurement with an error lower than 2% (Walley 1993) and with a very good spatial and temporal resolution. The method principle bases on the relation between the soil relative permittivity and the volumetric water content.

The permittivity is given by the formula

$$F = \frac{1}{\varepsilon}\frac{Q_1 Q_2}{r^2} \quad [4.8]$$

| | | |
|---|---|---|
| F | Attraction force between two electric charges | [N] |
| $Q_1$, $Q_2$ | Loads separated by a distance r in a uniform medium | [C] |

$\varepsilon$ = Permittivity

The permittivity of the air is equal to 1, that of the solid matrix oscillates between 2 and 5 while that of water is approximately 80. Thus, the soil water content variations affect in a dominating way the permittivity of this one. The technique consists in sending an electromagnetic impulse in a waveguide generally formed of two metal electrodes (sometimes three) of length L and analyzing the transit time T, either starting from the return signal of the impulse, or by measuring the transit time for various tensions(Auzet A.V., 1996). The 2 sensors consist of a thin-wall PVC body that is 2 cm in diameter and 15 cm long. At the top of the sensor are the two 10 cm long waveguides. The waveguides are stainless steel rods (diameter 2 mm) and separated by 16 mm. The region of influence of the sensor can be estimated as a cylinder having a length of 12 cm and a diameter of 5 cm. Outside of this region there is no noticeable interaction between the soil and the sensors electric field.
The propagation velocity C of an electromagnetic impulse along the waveguide is given by the relation:

$$C = \frac{c}{\sqrt{\varepsilon \mu_r}} \quad [4.9]$$

| | | |
|---|---|---|
| $c$ | Speed of light: $3 \times 10^8$ | [$m.s^{-1}$] |
| $\varepsilon$ | Permittivity | |
| $\mu_r$ | Magnetic permeability: it is equal to 1 for nonmagnetic materials | |

Knowing the length L of the waveguide, the distance covered is known (= 2l) and the soil permittivity can be deduced from the transfer time T.
in Tiergarten the soil surface water content was also measured by using TDR along a transect of 90cm by 60cm with a 10 cm X 10 cm resolution.

### *3.3.6. Statistical Analysis with Excel*

Within the framework of this study we measured temperature on our plot at various times but also the distribution of the water content with a spatial resolution of 10 cm X 10 cm. Firstly we calculated the average temperature according to this spatial resolution and we expect to note a significant dependence between this temperature and the water content at various times in particular early the morning, midday, in the twilight, and the night. The question is thus to know if the dependence observed is sufficient to reject the assumption that the indicator does not measure the soil water content effect. To check this assumption, we called upon a variance analysis for each moment. The variance analysis (ANOVA) is generally used for the data analysis of the experimental designs. It tests the assumption of the equality of the averages of several samples, in other words, the homogeneity of the averages of these samples. With this assumption H0, an alternative assumption H1 is associated, for which the averages of the samples are not all equal (the samples are not homogeneous). The variance analysis thus makes it possible to test the effect of one or several factors on the studied data, by comparison with a control sample. Its application is subjected to several conditions:

- Randomness and independent of the samples;
- Normal distribution;
- Equality of the variances.

In a practical way, through the ANOVA, one seeks to know if the variability observed in the data is only due randomly, or if there exist indeed significant differences between the samples, ascribable with the factors. The statistical test used is the F test of Fisher-Snedecor, which measures the report/ratio of the variance between classes (variance inside a group) with the variance within classes (variance between the groups).
The description was carried out by the ANOVA of the statistical software Excel of Microsoft Office. The probabilities (Pr > F) associated with the observation of the statistical test are limited to a threshold (alpha) $\alpha=0.05$, beyond whose the H0 assumption is rejected.

### *3.4. Results*

#### *3.4.1. Energy Balance Measurements Results*

With the radiation balance measurement, the short-wave and long-wave components of the Energy balance are seized within the range of 0,3.....60 µm. In this measure the sun – and sky radiation, artificial light sources radiation and surface reflection radiation are included. With this set we can measure also the wind velocity, wind direction, acoustic temperature, air temperature, relative humidity.

Figure 3.5 shows the energy balance diagram. With a wind velocity smaller than 1m/s, a air temperature between 18 and 32°c, and a relative humidity range 24 to 67%, the radiation balance varied from 0 to 602 W/m and it reached its maximum at 10:24 hours on the second day of the experiment.

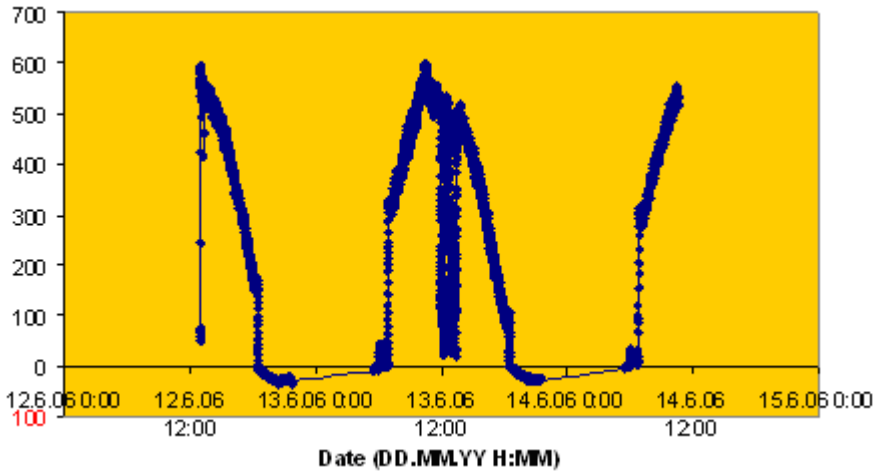


Figure 3.5: Energy balance diagram

#### *3.4.2. Water Content and Water Repellency Spatial Distribution*

Figure 3.7 shows the water content spatial distribution at 10 cm depth. At this depth the soil was a little bit dry and its gravimetric water content varied between 3% (g/g) and 11% (g/g). The gravimetric water content mean value per depth in Tiergarten indicate 9% (g/g) at the surface horizons which decreases till 8% (g/g)with the depth until 20 cm and after begin to increase till 11% (g/g). The tendency of the water content to the fall is done by successive steps. The maximum values close to the soil surface, about 20%, are not any more than 12% (g/g) at 20 cm depth. Below 20cm, the water content increases and reaches his maximum 25% (g/g) at 30cm depth.

The volumetric water contents lead to one conclusion:The gravimetric water content measurements and the volumetric water content measurements give completely comparable results at the soil surface.

Figure 3.6 shows the water repelllency spatial distribution at 10cm depth. At this depth, the soil exhibits a strong spatial distribution of extreme water repellent soil. And the water repellency was very variable. In most of areas the soil was extremely water repellent, while in the other areas the soil was slightly water repellent.

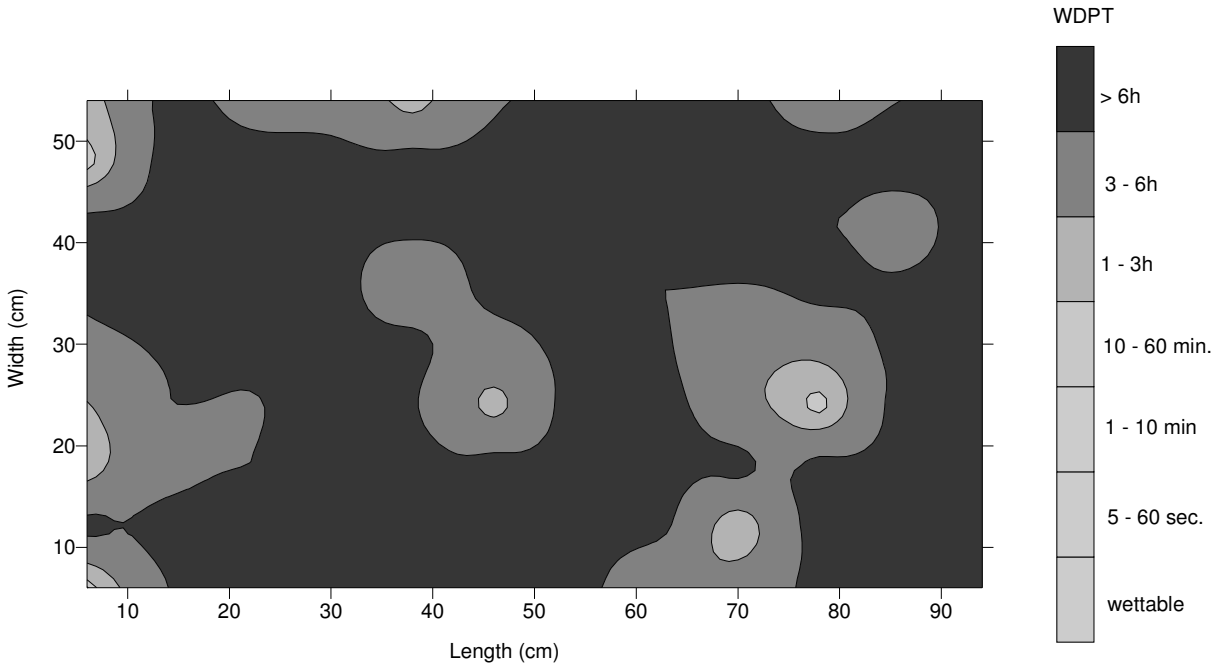


Figure 3.6: Water repellency spatial distribution at 10cm depth in Tiergarten

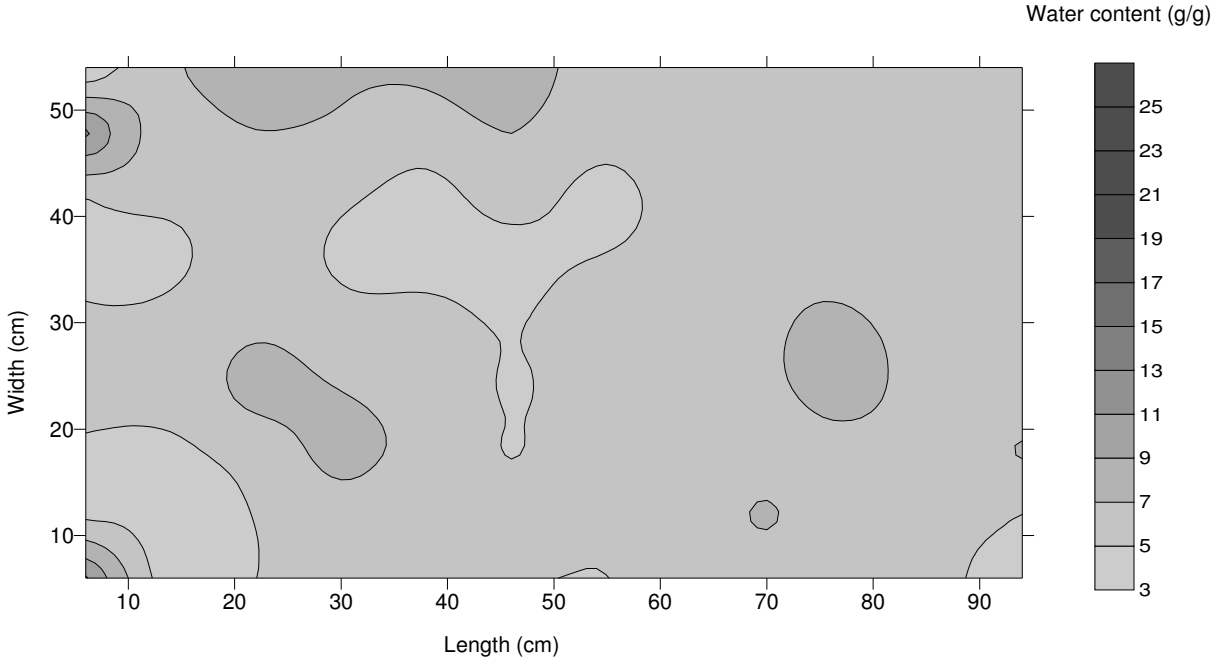


Figure 3.7: Water content spatial distribution at 10cm depth in Tiergarten

### *3.4.3. Brilliant Blue Flow Paths*

Figure 3.8 shows the flow path at 10cm depth in Tiergarten according the Brilliant Blue tracer. We found a small stained area of about 1 cm². That's why we had in this site a strong preferential flow according the depth marked by a percentage of flow paths lower than 1%. But it should be noted that the soil samples were in the majority extremely repellent. So there was no correlation between these two methods: WDPT test and Brilliant Blue experiment.

Figure 3.8: Flow path at 10cm depth in Tiergarten

### *3.4.4. Thermal Camera Results*

Figure 3.9 shows the evolution in time of the surface temperature at 5 points on our plot. At 6:45 the soil surface temperature is between 3℃ and 19℃ before the irrigation and between 9℃ and 18℃ after the irrigation. At 8:15 with the appearance of the first solar radiation on our plot, the temperatures rises from 2℃ to 27℃ before the irrigation and from 10℃ to 28℃ after irrigation. At 11 o'clock when the solar radiation cover completely the soil surface therefore the temperature go from 13℃ to 65℃ before irrigation and from 11℃ to 55℃. At 18 o'clock the shade begins to cover our plot and the soil surface temperature is between 2℃ and 54℃ before irrigation and between 13℃ and 39℃. At 21 o'clock the shade covers completely the topsoil and the soil surface temperature begins to be stabilized. Thus at 22:30 the surface temperature is between 2℃ and 20℃ before irrigation and between 5℃ and 22℃ after irrigation.

Figure 3.10 shows the statistical separation between surface temperature and water content at different times. The comparison between the soil surface temperature and the spatial soil water content distribution did not give a perfect equality but nevertheless showed no statistical relation between surface temperature and water content during the day and a strong correlation at the night.

Figure 3.11 shows the soil surface temperature before irrigation at (a) 22:30 (b) 11:30 and after irrigation at (d) 22:30 (e) 11:30 and differential image between 22:30 (night) and 06:45 (morning) (c) before irrigation (f) and after irrigation

As we see in Figure 3.12:which shows the soil surface temperature spatial distribution with 8X6cm resolution at 6:45 before irrigation and after irrigation and the water repellency spatial distribution at 5cm depth and also gravimetric water spatial distribution, the structure that we absorbed on the differentiated images was not constantly very significant and was not in connection with the water repellency spatial distribution. The analysis of the Table 3.2 which compare the canopy temperature variability and the Water content spatial distribution leads to no interpretable results. Since all the canopy temperature variability values exceed 2,7 which was our threshold refer of a hydrous stress it is appropriate to find another threshold value.

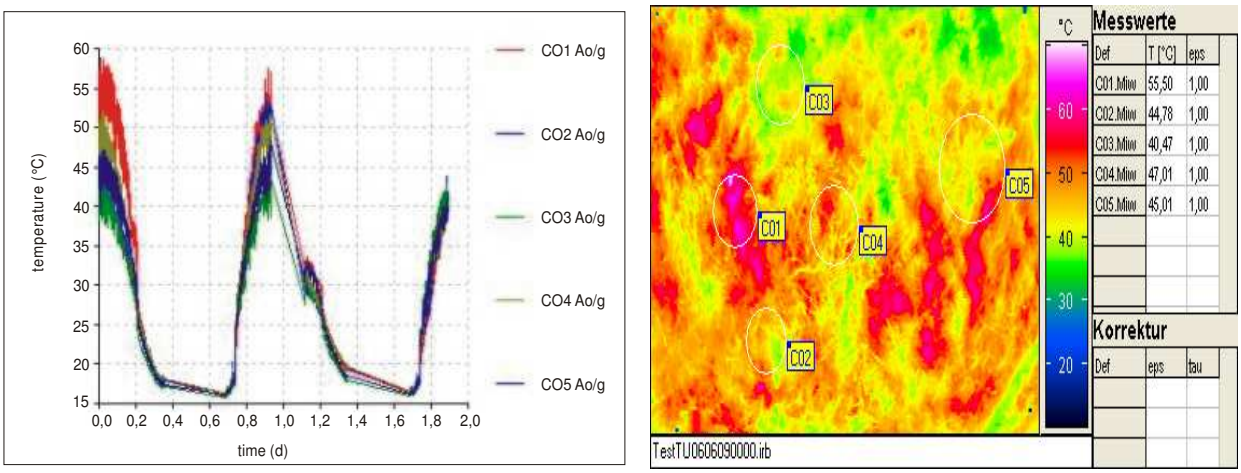


Figure 3.9: Temperature time diagram of 5 points at the soil surface

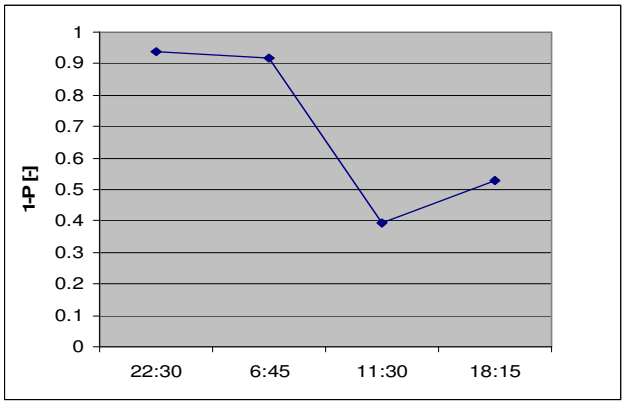


Figure 3.10: Statistical separation between surface temperature and water content at different times (p-values of the Anova test)

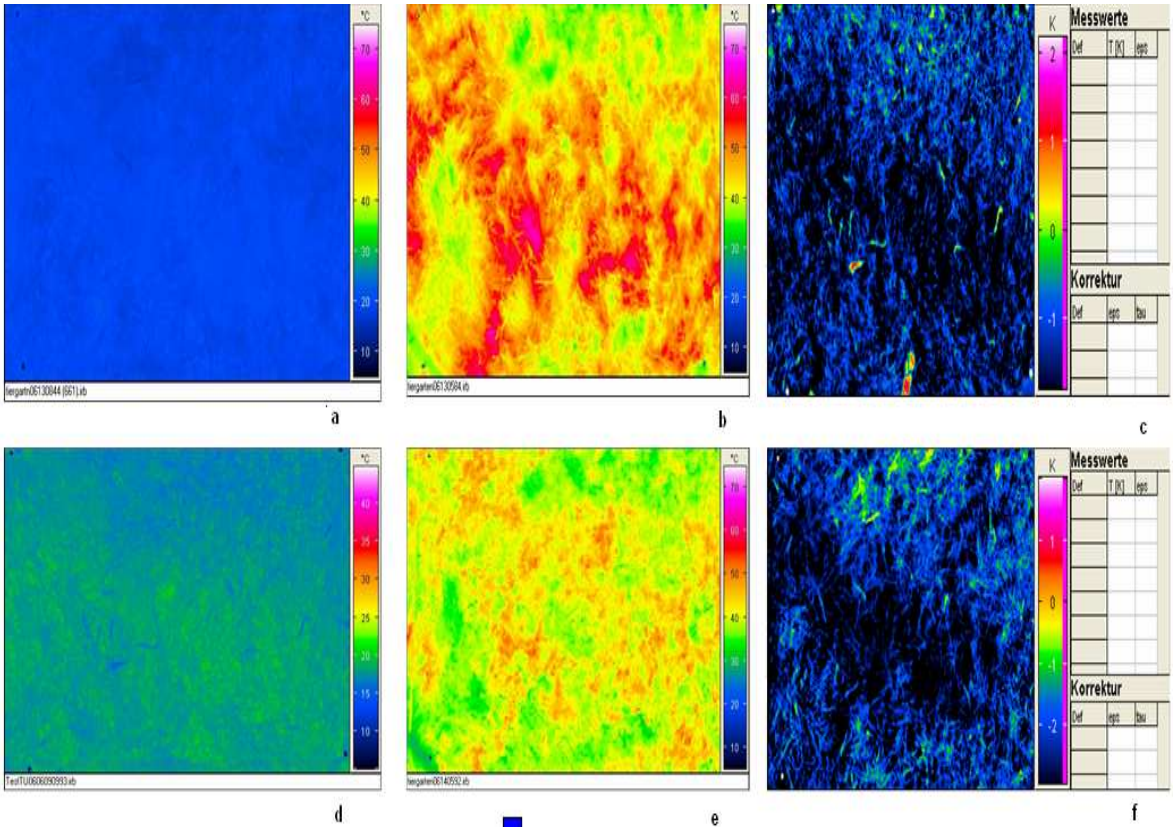


Figure 3.11: Soil surface temperature before irrigation at (a) 22:30 (b) 11:30 and after irrigation at (d) 22:30 (e) 11:30 and differential image between 22:30 (night) and 06:45 (morning) (c) before irrigation (f) after irrigation

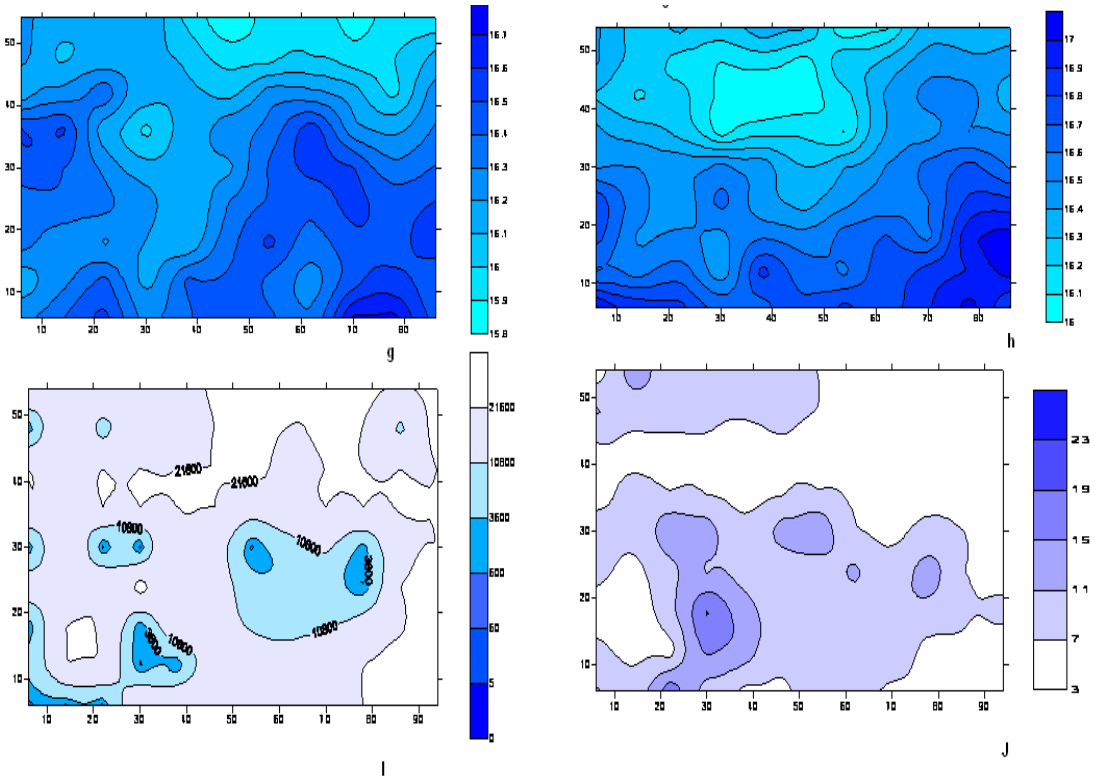


Figure 3.12: Spatial distribution with 8X6cm resolution of the Soil surface temperature at 6:45 before irrigation (g), after irrigation (h), and at 5cm depth WDPT (I) and gravimetric water (J)

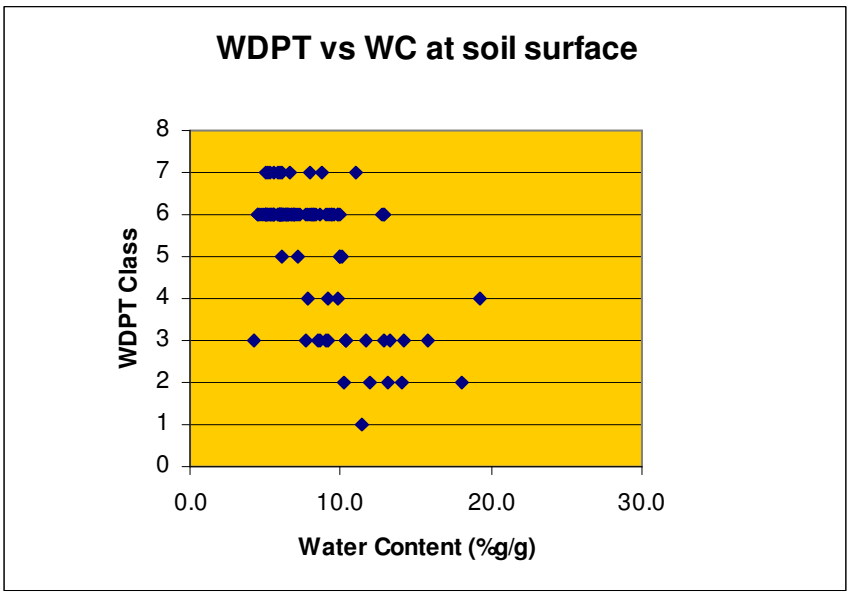


Figure 3.13 Comparison WDPT test and water content at soil surface

Table 3.2: Comparison canopy temeprature variability (CTV) and Water Content (WC) spatial distribution at 11:30

| | | | | | | | | | |
|---|---|---|---|---|---|---|---|---|---|
| CTV | | | | | | | | | |
| | 3.51 | 3.91 | 3.81 | 2.92 | 3.40 | 2.68 | 1.73 | 1.72 | 2.55 |
| WC | 7.80 | 8.20 | 7.10 | 7.00 | 9.10 | 6.6 | 7.3 | 6.9 | 7.5 |
| CTV | 4.65 | 4.05 | 3.04 | 2.98 | 2.68 | 3.95 | 4.23 | 3.53 | 3.55 |
| WC | 8.60 | 8.20 | 5.70 | 5.70 | 8.70 | 5.3 | 6.5 | 5.7 | 6.4 |
| CTV | 5.26 | 4.84 | 4.28 | 3.98 | 3.29 | 3.64 | 3.68 | 3.45 | 3.74 |
| WC | 7.40 | 8.50 | 8.80 | 6.30 | 7.90 | 13 | 5.3 | 6.4 | 5.1 |
| CTV | 5.17 | 2.78 | 3.40 | 4.13 | 3.54 | 4.84 | 3.37 | 4.48 | 3.31 |
| WC | 9.40 | 13.60 | 6.60 | 9.90 | 8.40 | 10.6 | 12.9 | 13 | 7.8 |
| CTV | 4.16 | 1.72 | 2.04 | 3.83 | 6.31 | 3.73 | 2.91 | 5.46 | 6.09 |
| WC | 7.70 | 16.00 | 10.30 | 9.90 | 7.00 | 8.6 | 9.5 | 7.8 | 5.6 |
| CTV | 2.91 | 2.56 | 4.30 | 4.53 | 3.47 | 3.88 | 2.45 | 2.81 | 3.73 |
| WC | 7.30 | 9.50 | 9.00 | 9.40 | 8.00 | 8.6 | 9.4 | 5.7 | 7 |

### *3.5. Conclusions*

The following conclusion focuses firstly on the experimental site of Berlin Buch, secondly on the numerical scenarios and finally on the experiences that have been garned in the Tiergarten park experiments.

**For the Buch Site**

At this site, we find water repellent structures only in the Ah Horizon, mostly in the first 50 cm of the topsoil. The soil water content in Berlin-Buch lies between 0,04 and 0,21 (g/g). The actual water repellency degree decreased according to the depth in both transects. In total 25% of the soil samples on the transect 2 were water repellent, whereas transect 1 showed approximately 30% repellent samples. The spatial distribution of the water repellency is similar to that of the water content. Also, it can be noted that up to 40 cm of depth, the percentage of flow paths equals approximately to the percentage of water repellent samples. This means that from the WDPT test, one can directly deduce the flow path spatial distribution.

The distribution of water repellent behavior was not directly correlated to the soil organic matter content, but areas without organic matter were not repellent. The Brilliant Blue experiment shows significant flow paths. In the topsoil, it is possible to determine the spatial water repellency distribution from the Brilliant Blue images. Wettable areas are colored by Brilliant Blue, water repellent ones are not. Nevertheless, below 50 cm, where there is no presence of water repellent samples, the Brilliant Blue experiment showed preferential flow

due to the gravitational flow of water. This preferential flow did not have any effect on the water content changes.

These preferential flows, in their turn, manage the "hydraulic cycle" of the soil. Because water is the main transport medium of solutes, the preferential flow due to the water repellency in the topsoil also influences the solute transport in the soil.

In combination with further measurements, the results can be used to detect the temporal dynamics of the spatial variability of water repellent areas. This will lead to a better understanding of the solute transport and water budget of water repellent sites.

**From the Numerical Scenarios**

The numerical scenarios lead to the following conclusions:

- The size of the wettable area as well as the initial water content difference between wet and dry soils influence the soil surface temperature, but not to a great extent.
- With increasing thickness of the soil layer above the wet and water repellent areas, the temperature differences at the soil surface decrease. The covering layer reduces the maximum between the differences in surface temperature above the wet and dry spots in the soil. If the wet and dry spots are covered with more than 10 cm soil, the influence on the soil surface temperature is almost negligible. In natural soils, the vegetation cover has to be taken into account as well.

The developed model integrates the majority of the thermal phenomena intervening with the exchange between the atmosphere and the soil. The numerical model does not calculate the water cycle. Since this soil thermal model takes many parameters into account, it can be adapted to any type of real situation. Nevertheless, the results show the possibility and the limits of detecting water repellent areas using thermography.

**For the Tiergarten Site**

At this site, a strong preferential flow marked by a small stained area of about 1 cm² was observed. In the remaining area, the majority of the soil samples were extremely repellent. The surface termperatures during the day were up to 65°C with a very high spatial variability. Different soil surface temperature structures during the day and during the night were detected. The comparison between these structures and the spatial soil water content distribution did not give a good correspondence. It was not possible to detected wetter and drier parts of the soil from the surface temperature. Nevertheless, water content and surface temperature correlated statistically significantly at night. This can be explained by the higher importance of the soil heat flux during night. The analysis of Table 3.2, which compares the canopy temperature variability and the water content spatial distribution, leads to no

interpretable results. All the CTV values exceed 2,7, the threshold referring to hydrous stress. Therefore, it is necessary to choose a different threshold value for water repellent sites.

## 4. Bibliography


Albert. R., Köhn. M., 1926. Investigations into the resistance of sandy soils to wetting. Proc. Int. Soc. Soil Sci. II, 139-145.

Auzet A.V. , Biron P., Bouchti A.,, Sanchez Perez J.M., Guth G., 1996, Mesures de l'humidité des sols à différentes profondeurs au moyen d'une sonde tube TDR : intercomparaison avec les mesures neutroniques. Atelier Instrumentation et Expérimentation. METEO -France / INSU, Toulouse, 6p

Bachmann, J., R. Horton, and R.R. van der Ploeg. 2001. Isothermal and nonisothermal evaporation from four sandy soils of different water repellency. Soil Sci. Soc. Am. J. 65:1599-1607

Bahrani, B., Mansell, R.S., Hammond, L.C., 1970. Wetting coefficients for water repellent sand. Soil and Crop Sci. Soc. Florida Proc. 30, 270-274.

Balland, V. and P. A. Arp (2005). "Modeling soil thermal conductivities over a wide range of conditions." Journal Of Environmental Engineering And Science 4(6): 549-558.

Bariou, R., Lecamus, D., and Henaff, L. F. 1985a, Dossiers de télédétection. Indices de végétation. Centre Régional de Télédétection, Université de Renne 2 - Haute Bretagne.

Bayliss. J.S. 1911. Observations on Marasmius oreades and Citocybe gigantean as parasitic fungi causing "fairy rings" J. Econ. Biol. 6, 111-132.

Berliner, P., Oosterhuis, D. M., and Green, G. C. 1984. Evaluation of the infrared thermometer as a crop stress detector. Agricultural and Forest Meteorology, Vol. 31, No. 3-4, pp. 219-230.

Berndtsson R. Persson H. Bahri A. Takuma K. Yasuda, H. Characterizing preferential transport during flood irrigation of a heavy clay soil using the dye vitasyn blau. Geoderma 100, 49-66, 2001.

Bickerman, I.J., 1941. A method of measuring contact angles. Ind. Engng. Chem. 13, 443-444

Bishay, B.G., Bakhati. H.K., 1976. Water Repellency of soils under citrus trees in Egypt and means of improvement. Agric. Resour. Rev. (Cairo) 54, 63-74.

Bond, R. D. (1964). "The influence of the microflora on the physical properties of soils. 11." Field studies on water repellent sands. Aust. J. Soil. Res 2: 123-31.

Brooks, S., Taylor, D., and Jardine, P. (1998). Thermodynamics of bromide exchange on ferrihydrite: implications for bromide transport. Soil Sci Soc Am J 62, 1275-1279.

Burkhardt M. Giesa S. Kasteel, R. and H. Vereecken. 2002 Characterization of feld tracer transport using high-resolution images. Am. Soil Sci. Society.

Campbell, G.S. 1985. Soil physics with BASIC. Elsevier, Amsterdam, the Netherlands.

Campbell, G.S., C. Calissendorf, and J.H. Williams. 1991. Probe for measuring soil specific heat using a heat-pulse method. Soil Sci. Soc. Am. J. 55 :291-293.

Chakrabarti, D.C. 1971. Investigation on erodibility and water sTable aggegates of certain soils of eastern Nepal. Indian Soc. Soil Sci. J. 19, 441-446.

Clarke P.J. Tate M.E. Oades J.M. Franco, C.M.M. (2000): Hydrophobic properties and chemical characterisation of natural water repellent materials in australian sands. J. Hydrol. 231-323,47-58.

Clay, D. E., Zheng, Z., Liu, Z., Clay, S. A., and Trooien, T. P. (2004). Bromide and Nitrate Movement through Undisturbed Soil Columns. J Environ Qual 33, 338-342.

Das, D.K., Das. B., 1972. Characterization of water repellency in Indian soils. Indian J. Agric. Sci. 42, 1099-1102.

De Rooj, G.H., de Vries, P.,1996. Solute leaching in a samdy soil with a water repellent surface layer: a simulation.Geoderma 70, 253-263.

De Vries, D.A. 1963. Thermal properties of soils. p. 210-235. In W.R. van.,Wijkw(ed) P.hysics of plant environment. John Wiley and Sons

Debano, L.F., 1975. Infiltration, evaporation and water movement as related to water repellency. In: Soil Conditionners: Proceedings of a symposium on Experimental Methods and Uses of Soil Conditionners (Moldenhauer, W.C., Program Chairman), November 15-16, 1973, Las Vegas, NV. Soil Sci. Soc. Am. Spec. Publ. Series 7, Madison, WI. pp. 155-163, 186pp.

Debano, L.F., Rice, R.M., 1973. Water repellent soils: their implications in forestry. J. For. 71, 220-223.

Debano, L.F., Savage, S.M., Hamilton, D.A., 1976. The transfer of heat and hydrophobic substances during burning. Soil Sci. Soc. Am. J. 40, 779-782.

Dekker L.W. Oostindie K. Ritsema C.J. Moral Garcia, F.J. Soil water repellency in the natural park of donana, southern spain. In: Ritsema, C.J., Dekker, L.W. (Eds.), Soil Water Repellency-Occurrence, Consequences and Amelioration. Elsevier, Amster-dam, pp. 121-127., 2003.

Dekker L.W. Ritsema C.J. Hendrickx J.M.H. Jaramillo, D.F. 2000 Occurrence of soil water repellency in arid and humid climates. J.Hydrol.231-232, 105-111.

Dekker L.W. Ritsema, C.J. 1998 Three-dimensional patterns of moisture, water repellency, bromide and ph in a sandy soil. J. Contam. Hydrol. 31, 295- 313,.

Dekker, L. W. and C. J. Ritsema (1994). "How Water Moves In A Water Repellent Sandy Soil.1. Potential And Actual Water Repellency." Water Resources Research 30(9): 2507-2517.

Dekker, L. W. and C. J. Ritsema (1995). "Finger-Like Wetting Patterns In 2 Water-Repellent Loam Soils." Journal Of Environmental Quality 24(2): 324-333.

Dekker, L. W. and C. J. Ritsema (1996). "Uneven moisture patterns in water repellent soils." Geoderma 70(2-4): 87-99.

Dekker, L. W. and C. J. Ritsema (1996). "Variation in water content and wetting patterns in Dutch water repellent peaty clay and clayey peat soils." Catena 28(1-2): 89-105.

Dekker, L. W. and C. J. Ritsema (1997). "Effect of maize canopy and water repellency on moisture patterns in a Dutch black plaggen soil." Plant And Soil 195(2): 339-350.

Dekker, L. W. and J. Bouma (1984). "Nitrogen leaching during sprinkler irrigation of a Dutch clay soil." Agricultural Water Management 9(1): 37-45.

Dekker, L.W., Ritsema, C.J., 1994. How water moves in a water repellent sandy soil: 1. Potential and actual water repellency. Water Resour. Res. 30, 2507-2517.

Dekker, L.W., Ritsema, C.J., Wendroth, O., Jarvis, N., Oostindie, K., Pohl, W., Larsson, M., Gaudet, J.-P., 1999. Moisture distributions and wetting rates of soils at experimental fields in the Netherlands, France, Sweden and Germany. J. Hydrol. 215, 4 - 22.

Doerr, S. H. (1998). "On standardizing the 'water drop penetration time' and the 'molarity of an ethanol droplet' techniques to classify soil hydrophobicity: A case study using medium textured soils." Earth Surface Processes And Landforms 23(7): 663-668.

Doerr, S.H., Shakesby, R.A., Walsh, R.P.D., 2000. Soil water repellency: its causes, characteristics and hydro-geomorphological significance. Earth-Sci. Rev. 51, 33-65.

Doerr, S.H., Thomas, A.D., 2003. Soil moisture: a controlling factor in water repellency? In: Ritsema, C.J., Dekker, L.W. (Eds.), Soil

Dyck, M. F., Kachanoski, R. G., and de Jong, E. (2003). Long-term Movement of a Chloride Tracer under Transient, Semi-Arid Conditions. Soil Sci Soc Am J 67, 471-477.

E. Zehe and H. Flüher. Slope scale variation of flow patterns in soil profiles. J. Hydrol.(Amsterdam) 247:116-132, 2001.

Emerson, W.W., 1967. A classification of soil aggegates based on theier coherence in water. Aust. J. Soil Res. 5, 47-57.

Flury, M. and H. Fluhler (1995). "Tracer Characteristics Of Brilliant Blue Fcf." Soil Science Society Of America Journal 59(1): 22-27.

Flury, M., Fluhler, H., Jury,W.A., Leuenberger, J., 1994. Susceptibility of soils to preferential flow of water: a field study. Water Resour. Res. 30, 1945-1954.

Flury, M.,Wai, N.N., 2003. Dyes as tracers for vadose zone hydrology. Rev. Geophys. 41, 966-1002.

Forrer, I., R. Kasteel, M. Flury, and H. Flühler (1999). Longitudinal and lateral dispersion in an unsaturated field soil. Water resources research 35 (10), 3049-3060.

Franco, C.M.M., Clarke, P.J., Tate, M.E., Oades, J.M., 2000. Hydrophobic properties and

chemical characterisation of natural water repellent materials in Australian sands. J. Hydrol. 231-323, 47-58.

Gaussorgues, G. 1999, La thermographie infrarouge : Principes, technologies, applications, Paris

Gerke, H.H., Hangen, E., Schaaf, W., Hqttl, R.F., 2001. Spatial variability of potential water repellency in a lignitic mine soil afforested with Pinus nigra. Geoderma 102, 255-274.

Gjettermann, B., Nielsen, K.L., Petersen, C.T., Jensen, H.E., Hansen, S., 1997. Preferential flow in sandy loam soils as affected by irrigation intensity. Soil Technol. 11, 139-152.

Gonzalez, R. C. and R. E. Woods (2002). Digital image processing. Upper Saddle River, New Yersey: Prentice Hall

Grunewald, J. 2000. DELPHIN 4.1–Documentation, Theoretical Fundamentals. TU Dresden

Hammel, K., Gross, J., Wessolek, G., and Roth, K. (1999). Two-dimensional simulation of bromide transport in a heterogeneous field soil with transient unsaturated flow. European Journal of Soil Science 50, 633-647.

Hangen E. Schaaf W. Hüttl R.F. Gerke, H.H. 2001 Spatial variability of potential water repellency in a lignitic mine soil afforested with pinus nigra. Geoderma 102, 255-274.

Hangen, E., H.H. Gerke, H. H., Schaaf, W., and Hüttl, R. F. (2005). Assessment of preferential flow processes in a forest-reclaimed lignitic mine soil by multicell sampling of drainage water and three tracers. Journal of Hydrology, 303, 1-4, 16-37.

Harris, R.F., Chesters, G., Allen, O.N., 1966. Dynamics of soil aggregation. Adv. Agron. 18, 107-169.Agron. 18, 107-169.

Heijs, A. W. J., C. J. Ritsema, et al. (1996). "Three-dimensional visualization of preferential flow patterns in two soils." Geoderma 70(2-4): 101-116.

Heijs, A. W. J., J. De Lange, et al. (1995). "Computed tomography as a tool for non-destructive analysis of flow patterns in macroporous clay soils." Geoderma 64(3-4): 183-196.

Henderson, G:S:, Golding, D.L., 1983. The effect of slash burning on the water repellency of forest soils at Vancouver, British Columbia. Can. J. For. Res. 13, 353-355.

Hendrickx, J.M.H., Dekker, L.W., Boersma, O.H., 1993. UnsTable wetting fronts in water reppellent field soils. J.Environ.qual.22,109-118.

Hendrickx, J.M.H., Dekker, L.W., van Zuilen, E.J., Boersma, O.H., 1988b, water and solute movement through a water repellent sand soil with grass cover in: wieringa, P.J., Bachelet, D.,(Eds.), Proceedings of a conference on the validation of flow and transport Models for unsaturated Zone. May 23-26,1988, Ruidoso, NM, New Mexico Research Report 88-SS-04, Department of Agronomy and Horticulture, New Mexico state universtity. Las Cruce, NM,pp.131-146,545pp.

Hillel, D., Berliner, P., 1974. Waterproofing surface-zone soil aggegates for water conservation. Soil Sci. 118, 131-135.

Hoffmann, C., 2002. Schwermetallmobilität und Risikopotentiale der Rieselfeldböden Berlin Buch, Bodenökologie und Bodengenese 35, Doctoral thesis, TU Berlin.

Holden N.M. Ward S.M. Collins J.F. Mooney, S.J. Morphological observations of dye tracer infiltration and by-pass flow in milled peat. Plant Soil 208, 167-178, 1999.

Humphrey, R. R. and R. J. Shaw (1957). "Paved drainage basins as a source of water for livestock or game." Journal of Range Management 10(2): 59-62.

Jaramillo, D.F., Dekker, L.W., Ritsema, C.J., Hendrickx, J.M.H.,2000. Occurrence of soil water repellency in arid and humid climates. J. Hydrol. 231-232, 105- 111.

John, P.H., 1978. Heat-induced water repellency in some new Zeland pumice soils. NZ J. Sci. 21, 401-407.

Kasteel, H. Papritz,. R. Fluehler, D. Luca, I. Forrer (2000): Quantifying dye tracers in soil profiles by image processing. Eur. J. Soil Sci. 51, 313-322.

Kasteel, R., Burkhardt, M., Giesa, S., and Vereecken, H. (2003). Characterization of Field Tracer Transport Using High-Resolution Images. Vadose Zone J. 4, 101-111.

Kenyon, S.A., 1929. The "ironclad" or artificial catchment. J. Dept. Agric. Victoria 27, 8-91.

Kildsgaard, J. and P. Engesgaard (2002). Tracer tests and image analysis of biological clogging in a two-dimensional sandbox experiment. Groundwater monitoring and remediation 22 (2), 60-67.

Kohne, J. M., and Gerke, H. H. (2005). Spatial and Temporal Dynamics of Preferential Bromide Movement towards a Tile Drain. Vadose Zone J 4, 79-88.

Kolyasev, F.E., Holodov, A.G., 1958. Hydrophobic earth as a means of moisture, thermal asnd electric insulation. In: Water and its conduction in Soils Highway Research Borad Special Report 40. National Academy Scienece. National Research Council Washington. DC. Pp. 298-307.

Koszinski, S., Quisenberry, V., Rogasik, H., and Wendroth, O. (2006). Spatial variation of tracer distribution in a structured clay field soil. Journal of Plant Nutrition and Soil Science 169, 25-37.

Kotchi, S., O., Detection du stress hydrique par thermographie infrarouge :application à la culture de la pomme de terre. Univ. Laval, 2004.

Kung, K.-J. S., Kladivko, E. J., Gish, T. J., Steenhuis, T. S., Bubenzer, G., and Helling, C. S.(2000). Quantifying Preferential Flow by Breakthrough of Sequentially Applied Tracers: Silt Loam Soil. Soil Sci Soc Am J 64, 1296-1304.

Lemon, E:R:, 1956. The potentialities for decreasing soil moisture evaporation loss. Soil Sci. Soc. Am. Proc. 20, 120-125.

Letey J, Osborn J, Pelishek RE. 1962a. Measurement of liquid-solid contact angles in soil and sand. Soil Science 93 : 149-153.

Letey J, Welch N, Pelishek RE, Osborn J. 1962b. Effect of wetting agents on irrigation of water-repellent soils. California Agriculture 16(12) : 12-13.

Letey, J., 1975. The use of non-ionic surfactants on soils. In: Soil Conditionners: Proceedings of a symposium on Experimental Methods and Uses of Soil Conditionners (Moldenhauer, W.C., Program Chairman), November 15-16, 1973, Las Vegas, NV. Soil Sci. Soc. Am. Spec. Publ. Series 7, Madison, WI. pp. 145-154, 186pp.

Letey. J 1968 Measurement of contact angle, water drop penetration time, and critical surface tension. In: DeBano, L.F., Letey, J.(Eds), proceedings of symposium on Water Repellent Soils, May 6-10, Riverside, CA, pp. 43-47, 354 pp.,.

Malicki, M. and W.Skierucha. 1989. A manually controlled tdr soil moisture meter operating with 300 ps rise-time needle pulse, Irrig. Sci., 10, 153-163.

Mallants, D., Jacques, D., Vanclooster, M.,Diels, J., Feyen, J., 1996. A stochastic approach to simulate water flow in a macroporous soil. Geoderma 70, 299-324.

Ma'shum, M., Farmer, V.C., 1985. Origin and assessment of water repellency of a sandy south Australian soil. Aust. J. Soil Res. 23, 623-626.

Mooney S.J. Lipsius, K. 2006 Using image analysis of tracer staining to examine the infiltration patterns in a water repellent contaminated sandy soil. Geoderma 136, 865-875.

Mooney, S.J., Holden, N.M., Ward, S.M., Collins, J.F., 1999. Morphological observations of dye tracer infiltration and by-pass flow in milled peat. Plant Soil 208, 167-178.

Moral Garcia, F.J., Dekker, L.W., Oostindie, K., Ritsema, C.J., 2003. Soil water repellency in the Natural Park of Donana, Southern Spain. In: Ritsema, C.J., Dekker, L.W. (Eds.), Soil Water Repellency-Occurrence, Consequences and Amelioration. Elsevier, Amsterdam, pp. 121-127.

Moran, M. S. 2000. Thermal infrared measurement as an indicator of plant ecosystem health. USDA-ARS Southwest Watershed Research Center. Tucson, Arizona.

Moran, M. S., Clarke, T. R., Inoue, Y., and Vidal, A. 1994. Estimating crop water deficitusing the relation between surface-air temperature and spectral vegetation index.Remote Sensing of Environment, Vol. 49, No. 3, pp. 246-263.

Morris, C., Mooney, S.J., 2004. A high resolution system for the quantification of preferential flow in undisturbed soil using observations of tracers. Geoderma 118, 133-143.

Mualem, Y. (1974). "A conceptual model of hysteresis." Water Resources Research 10(3) : 514-520.

Mussy, A., & Soutter, M. (1993). Physique du sol. Lausanne : Edition Tec et Doc.

Nakaya, N., 1982. Water repellency in soils. Jap. Agric. Res. Quart. 16(1), 24-28.

Nakaya, N., Motomura, S., Yokoi, H., 1977a. Some aspects on water repellency of soils. Soil

Sci. Plant Nutrition 23, 409-415.

Nehls, T., G. Jozefaciuk, Z. Sokolowska, M. Hajnos, and G. Wessolek (2006). Pore-system characteristics of pavement seam materials of urban sites. Journal of Plant Nutrition and Soil Science 169, 16-24.

Nielsen K.L. Petersen C.T. Jensen H.E. Hansen S. Gjettermann, B. 1997 Preferential flow in sandy loam soils as affected by irrigation intensity. Soil Technol. 11, 139-152,.

Öhrström M, Person P Y, Hamed and R. Berndtson. 2004 Characterizing unsaturated solute transport by simultaneous use of dye and bromide. J. Hydrol.(Amsterdam) 289 :23-35.

Penuelas, J., Save, R., Marfa, O., and Serrano, L. 1992. Remotely measured canopy temperature of greenhouse strawberries as indicator of water status and yield under mild and very mild water stress conditions. Agricultural and Forest Meteorology, Vol. 58, No. 1-2, pp. 63-77.

Philip, J.R., 1971. Limitations on scaling by contact angle. Soil Sci. Am. Proc. 37, 507-509.

Philip, J.R., 1975b. Stability analysis of infiltration. Soil Sci. Soc. Am. Proc. 39, 1042-1049.

Preferential flow processes in a forest-reclaimed lignitic mine soil by multicell sampling of drainage water and three tracers. Journal of Hydrology 303, 16-37.

Prusinkiewicz, A., kosakowski, A., 1986. The wettability of soil organic matter as the forming factor of the water properties of forest soils. Roczniki Gleboznawcze T. XXXVII, NR 1, S. 3-23, Warszawa.

Reichenberger, S., Amelung, W., Laabs, V., Pinto, A., Totsche, K.U., Zech, W., 2002. Pesticide displacement along preferential flow pathways in a Brazilian Oxisol. Geoderma 110, 63-86.

Richardson, J.L., 1984. Field observation and measurement of water repellency for soil surveyors. Soil Surv. Horizons 25(2), 32-36.

Rietveld, J., 1978. Soil non-wettability and its relevance as a contributing factor to surface runoff on sandy soils in Mali, Wageningen. Agricultural University. The Netherlands. 179pp.

Rietveld, M. R. (1978). “New Method For Estimating Regression Coefficients In Formula Relating Solar-Radiation To Sunshine.” Agricultural Meteorology 19(3) : 243-252.

Ritsema, C. J. and L. W. Dekker (1996). “Water repellency and its role in forming preferred flow paths in soils.” Australian Journal Of Soil Research 34(4) : 475-487.

Ritsema, C. J. and L. W. Dekker (1998). “Three-dimensional patterns of moisture, water repellency, bromide and pH in a sandy soil.” Journal Of Contaminant Hydrology 31(3-4) : 295-313.

Ritsema, C.J., Dekker, L.W., 1998. Three-dimensional patterns of moisture, water repellency, bromide and pH in a sandy soil. J. Contam. Hydrol. 31, 295- 313.

Schlenther, L., B. Marschner, C. Hoffmann and M. Renger. 1996. Ursachen mangelnder Anwuchserfolge bei der Aufforstung der Rieselfelder in Berlin-Buch - bodenkundliche Aspekte. Verh. Ges. Ökol. 25, 349-359.

Schreiner. O., Shorey. E.C. 1910 Chemical nature of soil organic mater. USDA Bureau Soils Bull. 74, 2-48.

Scott, D.F., 1988. Fire causes water repellency. In: de Klerk, J.(Ed.), Forestry News, Department of Environment Affairs, Private Bag X447. Pretoria 0001, republic South of Africa March 1988, pp. 18-20. 24pp.

Stoffregen H. 1998. Hydraulische Eigenschaften deponiespezifischer Materialien unter Berücksichtigung von Temperaturänderungen. Ph. D. diss. TU Berlin, Germany.

Taeumer, K., H. Stoffregen, and G. Wessolek (2005). Determination of repellency distribution using soil organic matter and water content. Geoderma 125, 107-115.

Tarara, J.M., and J.M. Ham. 1997. Measuring soil water content in the laboratory and field with dual-probe heat-capacity sensors. Agron. J. 89:535-542.

Taylor, D:H:, Blake, G.R., 1982. The effect of turfgrass thatch on water infiltration rates. Soil Sci. Soc. Am. J. 46, 616-619.

Tillman, R:W:, Scotter, D.R., Wallis, M.G., Clothier, B.E., 1989. Water repellency and its measurement by using intrinsic sorptivity. Aust. J. Soil Res. 27, 637-644.

Van Dam, J.C., J.H.M. Wösten, A. Nemes. 1996. Unsaturated soil water movement in hysteretic and water repellent field soils. J. Hydrol. 184, 153-173.

Vanderborght, J., Gahwiller, P., and Fluhler, H. (2002). Identification of Transport Processes in Soil Cores Using Fluorescent Tracers. Soil Sci Soc Am J 66, 774-787.

Vand't Woudt, B.D. 1968 Resistance to wetting under tropical and subtropical conditions. In: DeBano, L.F. Letey, J. (Eds), proceedings of a symposium on Water Repellent Soils, May 6-10, Riverside, CA. pp.7, 354pp..

Van't Woudt B.D. 1959 Particle coatings affecting the wettability of soils. J. Geophys. Res. 64, 263-267,.

Vogel H.J. Roth K. Kasteel, R. 2002 Effect of non linear adsorption on the transport behaviour of brilliant blue in a feld soil. Eur J. Soil Sci.53, 231-240.

Walley, W.R. 1993. Considerations on the use of time-domain reflectometry (TDR) for measuring soil water content. J. Soil Sci. 44:1–9.

Wallis, M. G., D. R. Scotter (1991). "An Evaluation Of The Intrinsic Sorptivity Water Repellency Index On A Range Of New-Zealand Soils." Australian Journal Of Soil Research 29(3): 353-362.

Watson, C.L. and Letey, J., 1970. Indices for characterizing soil-water repellency based upon contact angle-surface tension relationships. Soil Sci. Soc. Am. Proc. 34, pp. 841-844.

Watson, C.L., Letey, J., 1970. Indices for characterizing soil-water repellency based upon contact angle-surface tension relationships. Soil Sci. Soc. Am. Proc. 34, 841-844.

Welch, S.M., G.J. Kluitenberg, and K.L. Bristow. 1996. Rapid numerical estimation of soil thermal properties for a broad class of heat pulse emitter geometries. Meas. Sci. Technol. 7:932-938.

Wells, W.G. II, 1987. The effects of fire on the generation of debris flows in southern California. Rev. Engng. Geol. VII, 105-114.

Wiegand, C. L., Nixon, P. R., and Jackson, R. D. 1983. Drought detection and quantification by reflectance and thermal responses. Agricultural Water Management, Vol. 7, No. 1-3, pp. 303-321.

Yasuda, H., Berndtsson, R., Persson, H., Bahri, A., Takuma, K., 2001. Characterizing preferential transport during flood irrigation of a heavy clay soil using the dye Vitasyn Blau. Geoderma 100, 49-66.

Yuan, G., Luo, Y., Sun, X., and Tang, D. 2004. Evaluation of a crop water stress index fordetecting water stress in winter wheat in the north china plain. Agricultural Water Management, Vol. 64, No. 1, pp. 29-40.

Zaslavsky, D., Sinai, G., 1981. Surface Hydrology. IV. Flow in sloping, layered soil. J. hydraul. Dev. Am. Soc. Civil Engng. 107, 53-64.